



Impact of NO_x on secondary organic aerosol (SOA) formation from α -pinene and β -pinene photo-oxidation: the role of highly oxygenated organic nitrates

5 Iida Pullinen^{1,4}, Sebastian Schmitt^{1,5}, Sungah Kang¹, Mehrnaz Sarrafzadeh^{1,3,6}, Patrick Schlag^{1,7},
Stefanie Andres¹, Einhard Kleist², Thomas F. Mentel¹, Franz Rohrer¹, Monika Springer¹, Ralf
Tillmann¹, Jürgen Wildt^{1,2}, Cheng Wu^{1,8}, Defeng Zhao^{1,9}, Andreas Wahner¹ and Astrid Kiendler-Scharr¹

¹Institute for Energy and Climate Research, IEK-8, Forschungszentrum Jülich, 52425, Jülich, Germany

²Institute of Bio- and Geosciences, IBG-2, Forschungszentrum Jülich, 52425, Jülich, Germany

³Centre for Atmospheric Chemistry, York University, 4700 Keele St., Toronto, ON M3J 1P3, Canada

10 ⁴Present address: Department of Applied Physics, University of Eastern Finland, Kuopio, Finland

⁵Present address: TSI GmbH, 52068 Aachen, Germany

⁶Present address: PerkinElmer, 501 Rowntree Dairy Rd, Woodbridge, ON, L4L 8H1, Canada

⁷Present address: Shimadzu Deutschland GmbH, 47269 Duisburg, Germany

⁸Present address: Department of Environmental Science, Stockholm University, 11418 Stockholm, Sweden

15 ⁹Present address: Dept. of Atmos. and Oceanic Sci. & Inst. of Atmos. Sci., Fudan University, Shanghai, 200438, China

Correspondence to: Thomas F. Mentel (t.mentel@fz-juelich.de)

Abstract. The formation of organic nitrates (ON) in the gas phase and their impact on mass formation of Secondary Organic Aerosol (SOA) was investigated in a laboratory study for α -pinene and β -pinene photo-oxidation. Focus was the elucidation
20 of those mechanisms that cause the often observed suppression of SOA mass formation by NO_x, and therein the role of highly oxygenated multifunctional molecules (HOM). We observed that with increasing NO_x a) the portion of HOM organic nitrates (HOM-ON) increased, b) the fraction of accretion products (HOM-ACC) decreased and c) HOM-ACC contained on average smaller carbon numbers.

Specifically, we investigated HOM organic nitrates (HOM-ON), arising from the termination reactions of HOM peroxy radicals with NO_x, and HOM permutation products (HOM-PP), such as ketones, alcohols or hydroperoxides, formed by other
25 termination reactions. Effective uptake coefficients γ_{eff} of HOM on particles were determined. HOM with more than 6 O-atoms efficiently condensed on particles ($\gamma_{eff} > 0.5$ in average) and for HOM containing more than 8 O-atoms, every collision led to loss. There was no systematic difference in γ_{eff} for HOM-ON and HOM-PP arising from the same HOM peroxy radicals. This similarity is attributed to the multifunctional character of the HOM: as functional groups in HOM
30 arising from the same precursor HOM peroxy radical are identical, vapor pressures should not strongly depend on the character the final termination group. As a consequence, the suppressing effect of NO_x on SOA formation cannot be simply explained by replacement of terminal functional groups by organic nitrate groups.

The fraction of organic bound nitrate (OrgNO₃) stored in gas-phase HOM-ON appeared to be substantially higher than the fraction of particulate OrgNO₃ observed by aerosol mass spectrometry. This result suggests losses of OrgNO₃ for
35 organic nitrates in particles, probably due to hydrolysis of OrgNO₃ that releases HNO₃ into the gas phase but leaves behind the



organic rest in the particulate phase. However, the loss of HNO_3 alone, could not explain the observed suppressing effect of NO_x on particle mass formation from α -pinene and β -pinene.

We therefore attributed most of the reduction in SOA mass yields with increasing NO_x to the significant suppression of gas-phase HOM-ACC which have high molecular mass and are potentially important for SOA mass formation at low NO_x conditions.

1 Introduction

Secondary organic aerosol (SOA) constitutes a substantial fraction of ambient aerosol. It is formed from oxidation products of volatile organic compounds (VOC) and known to adversely affect visibility, climate and human health (Hallquist et al., 2009). With annual emissions around 1100 Tg, the biosphere is the strongest source of tropospheric VOC (Guenther et al., 2012) and thus, SOA formation from biogenic VOC is of high importance. Despite the outstanding role of biogenic VOC by amount and reactivity, anthropogenic trace gases affect SOA formation and possible anthropogenic enhancement effects were found in laboratory and field studies (e.g., De Gouw et al., 2005; Carlton et al., 2010; Emanuelsson et al., 2013; Hoyle et al., 2011; Spracklen et al., 2011; Worton et al., 2011; Glasius et al., 2011; Xu et al., 2015a; Shilling et al., 2013). Examples of important anthropogenic trace gases are NO and NO_2 , which together form the NO_x family. NO_x controls the atmospheric HO_x cycle thus the oxidation cycle of VOC, it efficiently reacts with peroxy radicals and affects SOA formation. In a number of studies the role of NO_x in the formation of SOA mass was investigated (Pandis et al., 1991; Presto et al., 2005; Kroll et al., 2006; Zhang et al., 2006; Ng et al., 2007; Kim et al., 2012; Eddingsaas et al., 2012; Han et al., 2016; Sarrafzadeh et al., 2016; Stirnweis et al., 2017). In most cases it was observed that NO_x decreased mass yields of SOA formation and the effects were generally attributed to impacts of $\text{RO}_2 + \text{NO}$ reactions. Sarrafzadeh et al. (2016) show that parts of the apparent suppression of SOA yields from β -pinene by NO_x was due to the role of NO_x in the HO_x cycle. As mass yields of SOA formation from α -pinene and β -pinene photo-oxidation depend on the actual OH concentrations, NO_x affects SOA formation also via decreasing or increasing OH concentrations according to reactions R1 and R2:

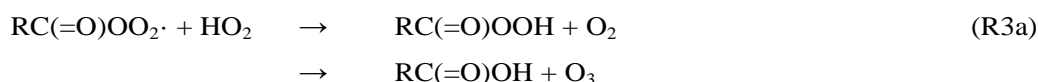


Since NO_x is inhibiting new particle formation (NPF, Wildt et al., 2014), the absence of particles in the presence of NO_x prevents formation of sufficient particle surface where low volatile compounds could condense on. Then other sinks gain in importance for low volatile compounds as dry deposition in the environment or wall losses in chamber experiments. In order to circumvent these effects, Sarrafzadeh et al. (2016) used seed particles always providing sufficient surface for the gas phase precursors of SOA mass to condense on and kept the OH concentrations constant. As a result the remaining effect of NO_x on



SOA mass formation from β -pinene and on SOA yields was only moderate. Generally, in absence of NO_x , peroxy radicals ($\text{RO}_2\cdot$) mainly react with other peroxy radicals (including the $\text{HO}_2\cdot$ radical) whereby termination products like hydroperoxides, ketones, alcohols, carboxylic acids and percarboxylic acids are produced. In reactions between peroxy radicals also alkoxy radicals are formed, which continue the radical chain (reactions R3 and R4):

5

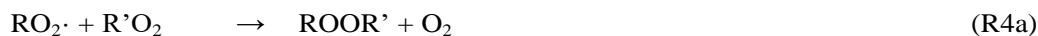


10



As observed in several studies with highly oxygenated multifunctional molecules (HOM, e.g. Ehn et al., 2012; Ehn et al., 2014; Mentel et al., 2015; Berndt et al., 2018a, b) accretion products can be formed in peroxy - peroxy radical reactions:

15



In laboratory studies HOM accretion products can contribute significantly to SOA yields (McFiggans et al., 2019).

The presence of NO_x opens new pathways with large reaction rates and production of organic nitrates (R5), including PAN-like compounds (R6). Furthermore, substantial amounts of alkoxy radicals (R7) are formed:



25

From reactions R3 to R7 it is obvious that the chemically stable products of peroxy radicals will have different termination groups under low and high NO_x conditions: while hydroperoxides, ketones, carboxylic acids etc. predominate at low NO_x conditions, organic nitrates (ON), including PAN like compounds become more important at high NO_x conditions.

Recent studies demonstrated the dominant role of HOM in SOA mass formation (Ehn et al., 2014; Jokinen et al., 2015; Mutzel et al., 2015; Zhang et al., 2017; McFiggans et al., 2019). HOM are formed by addition of molecular oxygen to alkyl radicals that are formed after H-migration in peroxy- or in alkoxy radicals. Due to a relative long lifetime of peroxy radicals such H-shifts with addition of molecular oxygen can appear several times in sequential steps and is therefore termed autoxidation (Crouse et al., 2011; Rissanen et al., 2014; Mentel et al., 2015). This process leads to highly oxygenated multifunctional peroxy radicals (HOM peroxy radicals). If the respective HOM is formed exclusively via autoxidation of



peroxy radicals, the HOM moieties are very likely multiple hydroperoxides (Rissanen et al., 2014; Berndt et al., 2016). If there are intermediate steps via alkoxy radicals there maybe also alcohol groups (Mentel et al., 2015). As HOM are low volatile organic compounds (LVOC) or even extremely low volatile organic compounds (ELVOC), they substantially contribute to mass formation of particles and support NPF (Ehn et al., 2014; Bianchi et al., 2016; Kirkby et al., 2016; Tröstl et al., 2016; Lehtipalo et al., 2018). All experimental evidence show that HOM peroxy radicals terminate with similar rates as less functionalized peroxy radicals (Berndt et al., 2016; Ehn et al., 2017; Bianchi et al., 2019). At low NO_x levels, HOM hydroperoxides, HOM alcohols, HOM carboxylic acids and HOM percarboxylic acids as well as HOM ketones are expected from the termination step and in addition HOM accretion products (HOM-ACC).

At high NO_x levels HOM-ON become important termination products. In addition HOM-ACC products are suppressed (Lehtipalo et al., 2018) and shifted to smaller C-numbers. The effect of NO_x on HOM-RO₂ chemistry is important step for understanding of impact of NO_x on SOA formation. In this paper we analyze two aspects of the effect of NO_x which are important for SOA yield: the formation and the volatility of HOM-ON as well as the suppression of HOM accretion products.

2 Experimental

2.1 Description of the chamber setup and experiments

Experiments were conducted in the Jülich Plant Atmosphere Chamber (JPAC, Mentel et al., 2009; 2013). The actual setup of the chambers was already described in several recent publications (Ehn et al., 2014; Wildt et al., 2014; Mentel et al., 2015; Sarrafzadeh et al., 2016). A 1.45 m³ chamber made of borosilicate glass and set up in a climate-controlled housing was used for these experiments. The chamber was operated as a continuously stirred tank reactor. About thirty-one liters of purified air per minute were pumped through the chamber resulting in a residence time of approximately 46 min. Mixing was ensured by a fan and the mixing time was about 2 minutes. The inlet flow was provided by two about equal purified air streams with one of them containing ozone and water vapor. In the second stream the VOC of interest was introduced from a diffusion source. Temperature (16 ± 1 °C) and relative humidity (63 ± 2%) inside the chamber were held constant over the course of the experiments.

The chamber was equipped with several lamps. Two discharge lamps (HQI400 W/D, Osram) served to simulate the solar light spectrum. Twelve UVA discharge lamps (Philips, TL 60 W/10-R, 60W, λ_{max} = 365 nm) provided the photolysis of NO₂ with a photolysis frequency J(NO₂) of ~3.3 × 10⁻³ s⁻¹. An UVC lamp (Philips, TUV 40W, λ_{max} = 254 nm) was used to produce OH radicals by ozone photolysis and reaction of O¹D atoms with water vapor. This lamp was housed in a quartz tube across the chamber diameter and parts of the lamp were shielded by movable glass tubes. By altering the gap between these glass tubes, the photolysis frequency for ozone, J(O¹D) and therewith the OH production rate could be adjusted. During most of the experiments described here, J(O¹D) was about 2.9 × 10⁻³ s⁻¹. The photolysis frequencies J(NO₂) and J(O¹D) (as function of the TUV gap) were determined experimentally by actinometry with NO₂ and O₃ in the chamber. Gas-phase compounds were



measured such as ozone (O_3 , UV-absorption, Thermo Environmental 49), nitrogen monoxide (NO, chemiluminescence, Eco Physics, CLD 770 AL ppt), and nitrogen dioxide (NO_2 , chemiluminescence after photolysis, Eco Physics, PLC 760). Water vapor concentrations were measured by dew point mirror (TP- 2, Walz).

We used the monoterpenes α -pinene and β -pinene (both Aldrich, 95% purity) as SOA precursors. The monoterpenes (MT) were measured either by gas chromatography mass spectrometry (GC-MS; Agilent GC-MSD system with HP6890 GC and 5973 MSD) or by proton transfer reaction mass spectrometry (PTR-MS; Ionicon, Innsbruck, Austria). Both devices were switched between the outlet and the inlet of the chamber in order to quantify concentrations in the chamber and to determine the VOC source strength.

To provide NO_x to the photochemical system we added NO_2 (Linde, 100 ppm NO_2 in nitrogen) in the β -pinene experiments or NO (90 ppm in nitrogen) in the α -pinene experiments to the VOC containing air stream. In case of NO_2 addition, a fraction of the added NO_2 was converted to NO due to the NO_2 photolysis. In case of NO addition, the major portion of the added NO was converted to NO_2 by reaction with O_3 . We adjusted the O_3 addition such that a steady state $[O_3]$ within a range of 60 - 90 ppb was achieved. We observed memory effects for NO_x probably due to Teflon parts (tubing, fan) in the chamber. In particular after experiments at high NO_x concentrations residual NO_x appeared in the chamber on the next day when switching on the TUV lamp. To minimize the memory effect, the chamber was operated without NO_x for one day between the NO_x experiments. The background NO_x concentration was around 300 ppt. When adding NO_x , its initial concentration, $[NO_x]_0$ was between 5 and 150 ppb and thus substantially above the background levels.

The results presented here were obtained at steady state conditions when all physical and chemical parameters were constant or in steady state, respectively. To indicate reference to steady state we mark the concentrations of MT and NO_x with the subscript "SS". To allow better comparison to literature data we refer in some instances to the initial concentrations $[NO_x]_0$, $[\alpha\text{-pinene}]_0$, and $[\beta\text{-pinene}]_0$, indicated by subscript "0", which are in our case input concentrations.

The OH concentrations were calculated from the decay of the respective MT in the chamber (Eq.2).

$$\frac{d[VOC]}{dt} = \frac{F}{V} ([VOC]_0 - [VOC]) - (k_{OH} \cdot [OH] + k_{O_3} \cdot [O_3]) \cdot [VOC] \quad (1)$$

$$[OH]_{SS} = \frac{\frac{F}{V} \frac{[VOC]_0 - [VOC]_{SS}}{[VOC]_{SS}} - k_{O_3} \cdot [O_3]_{SS}}{k_{OH}} \quad (2)$$

Equation (1) describes mass balance of the MT in the chamber and Eq. (2) results from Eq. (1) under steady state conditions when $d[VOC]/dt = 0$. In Eq. (1) and (2), V is the volume of the chamber, F is the total air flow through the chamber, $[VOC]_0$ and $[VOC]$ are the concentrations of the VOC under investigation in the inlet air and in the chamber, respectively. k_{OH} and k_{O_3} are the respective rate coefficients for the reactions of the VOC with OH and with O_3 . In one case, where the concentration of β -pinene was altered during the experiment, m-xylene was added as a tracer for [OH].



Rate constants used for the determinations of [OH] were: $k_{OH} = 5.37 \cdot 10^{-11}$, $7.89 \cdot 10^{-11}$, and $2.3 \cdot 10^{-11} \text{ cm}^3 \text{ s}^{-1}$ for α -pinene, β -pinene, and m-xylene, respectively (Atkinson 1997; Atkinson 1994). At typical conditions with $[O_3] \sim 60\text{-}100 \text{ ppb}$ and $[OH] \sim 3 \cdot 10^7$ the consumption of α -pinene by O_3 ($k_{O_3} = 8.7 \cdot 10^{-17} \text{ cm}^3 \text{ s}^{-1}$) was about 5% compared to that by OH. α -pinene losses due to ozonolysis were therefore neglected for the determination of [OH]. As β -pinene has an even lower ozonolysis rate constant ($k_{O_3} = 1.5 \times 10^{-17} \text{ cm}^3 \text{ s}^{-1}$, Atkinson, 1997), and m-xylene does not react with O_3 ($k_{O_3} < 1.5 \times 10^{-21} \text{ cm}^3 \text{ s}^{-1}$, Atkinson et al., 1994) ozonolysis reactions were also neglected for OH estimations using these VOC. The overall uncertainty in OH concentration was estimated to be about 20% (Wildt et al., 2014).

Our results were obtained in different types of experiments. An overview of the performed experiments with their starting conditions is given in Table 1. Details of the procedures applied during individual experiments are described in the respective sections. Three experiment series (1-3) were conducted to characterize gas phase products and experiment series 4 was conducted to characterize the particle phase. In the first experiment we estimated the molar yield of all organic nitrates (ON) independent of their contribution to particle formation. This was made at the example of β -pinene at one NO_x concentration (see section 3.1). Experiment series 2 were performed to determine the fraction of HOM organic nitrates at the total amount of HOM. Both monoterpenes were used with several NO_x levels as indicated (see section 3.3). In experiment series 3 we determined effective uptake coefficients for HOM at a low and at a high NO_x level for HOM-ON and other HOM termination products (see section 3.4). These experiments were performed with seed particles (ammonium sulfate). In the last experiment series 4 we characterised the amount of nitrate bound to organics in particles for comparison with the amount of organic bound nitrate in those HOM-ON that efficiently contribute to particle formation.

2.2 Determination of highly oxygenated molecules (HOM)

Highly Oxygenated Molecules (HOM) were measured by a Chemical Ionisation Mass Spectrometer operated with nitrate as reagent ion (NO_3^- -CIMS, Jokinen et al., 2012). First we determined that the relative transmission curve of our NO_3^- -CIMS was flat (supplement section S1.1). This indicates that detection of HOM within the mass range from $\sim 230 \text{ Da}$ to $\sim 600 \text{ Da}$ is nearly mass independent. So far no absolute calibration method exists for HOM. However, the charging efficiency for HOM is near to the kinetic limit like that for sulfuric acid (Ehn et al., 2014; Kirkby et al., 2016). Thus, the sensitivity of the NO_3^- -CIMS to HOM is supposedly similar to that of sulfuric acid. We therefore calibrated our NO_3^- -CIMS to sulfuric acid and used the calibration coefficient for the HOM, too (see supplement section S1.2). Applying the sulfuric acid calibration coefficient to the HOM we investigated the mass balance between condensing HOM and formed particle mass which was closed within a factor of 2 (see supplement section S1.3). It is also likely that the sensitivity of the NO_3^- -CIMS does not depend much on the functional group formed in the final termination step. This assumption is reasonable as HOM formed by autoxidation contain several hydroperoxy groups or a mixture of hydroxy and hydroperoxy groups, if they are formed via the alkoxy peroxy path (Mentel et al., 2015). Furthermore, a good agreement of the fraction of organic nitrates on the total reaction products of β -pinene (see section 3.1) and the fraction of HOM-ON of the total HOM gives us confidence that the uncertainty induced by this assumption does not affect much the main conclusions.



This all together with the quantum mechanical results of same sensitivity for HOM containing 6 or more O-atoms (Hytinen et al., 2017) gave us confidence that concentrations of HOM with 6 or more O atoms were determined with the same sensitivity to an uncertainty of less than a factor of two.

5 In summary, we used the calibration coefficient for H_2SO_4 to calculate HOM concentrations. We further concluded a same sensitivity for the detection of all HOM including accretion products when they contained 6 and more O-atoms. These conclusions are supported by observations of Breitenlechner et al. (2017) who found that, once the HOM contains more than 5 O-atoms, the sensitivity is to a good approximation independent of the number of O-atoms. The sensitivity of the NO_3^- -CIMS is unclear for compounds containing less than 5 O-atoms (Rissanen et al., 2014; Hyttinen et al., 2017; Riva et al.,
10 2019). However, as will be shown in section 3.4, HOM with less than 5 O atoms are of minor importance for particle mass formation, hence we will neglect them and this will not contribute much uncertainty on our results.

Identification of molecular formulas for individual HOM was obtained using high resolution spectra (resolution power ≈ 4000) as described in the supplement section S2. In case of HOM spectra from β -pinene photo-oxidation we found many not-fully-resolved double peaks from the overlapping of C_{10} , C_9 , and C_8 progressions. The mass spectra of α -pinene HOM in
15 general consisted of singular peaks, i.e. they were quite well resolved. Figure S5 in supplement section S2 shows, how HOM- RO_2 and HOM-ON were separated with increasing NO_x .

The observed concentration of gas-phase HOM depends on the OH concentration and the condensation sink provided by newly forming particles. Adding to or removing NO_x from a given photochemical system directly impacts [OH] by reactions R1 and R2. NO_x furthermore suppresses new particle formation (Wildt et al., 2014) which leads to a decreasing
20 condensation sink for HOM with increasing NO_x . The actual OH concentration affects the actual turnover of the precursor, thus the actual production of RO_2 and HOM, while the actual condensational sink leads to condensational loss of HOM. Both factors change the observed HOM gas-phase mixing ratio and can superimpose the impacts of NO_x on peroxy radical chemistry itself. In order to separate the chemical impacts of NO_x on HOM peroxy radical chemistry, we needed to take out the effects of [OH] and condensational sink as much as possible. This was achieved by normalizing the HOM mixing ratio to
25 particle free conditions and to a certain reference oxidation rate. The procedure is described in detail in supplement section S3.

2.3 Particle-phase measurements

To characterize the particle phase we used a condensation particle counter (CPC, TSI 3783), a scanning mobility particle
30 sizer (Electrostatic classifier TSI 3080, including a differential mobility analyzer TSI 3081 and a CPC TSI 3025A) and an aerosol mass spectrometer (AMS, Aerodyne HR-ToF-MS, modified for application on a Zeppelin airship, (Rubach, 2013)). In the AMS the aerosol particles were vaporized at 600 °C and ionized by electron impact ionization at 70 eV. The AMS was routinely operated in V-mode in two alternating modes: 1 min. MS mode to measure the chemical composition and 2 min.



PToF mode. Only MS mode data were analyzed here. We separated organic and inorganic particulate nitrate and determined the amount of OrgNO₃ by the NO₂⁺/NO⁺ method for AMS (Farmer et al., 2010; Kiendler-Scharr et al., 2016). SOA yields were determined as described in Sarrafzadeh et al. (2016). For determining mass yields, the particle mass formed during steady state conditions was divided by the mass of the consumed MT, which is the difference between inlet and outlet concentration:

$$Y = \frac{\text{produced particle mass}}{\text{BVOC consumption}} \quad (3)$$

During measurements of particle mass, the mean diameter of particles was above 100 nm. As the loss rates of such particles on the chamber walls were low, they were neglected. Losses of oxidized SOA precursors to the chamber walls were considered by applying the correction function given by Sarrafzadeh et al. (2016). This function describes the ratio of wall losses over the sum of wall losses and losses on particles. For the data given here, the correction factors were between 1.5 and 2.1.

2.4 Determination of effective uptake coefficients

We operated our chamber as a continuously stirred tank reactor (CSTR) in a flow through mode with a well-mixed core of the chamber. HOM lost at the chamber walls must diffuse through the laminar boundary layer at the chamber walls. In the chamber with no aerosols present, the walls constitute the major sink of HOM. In this case the observed steady state concentration is determined to a very good approximation only by the production rate and the wall loss rate. When seed aerosol is added or new particles are formed, the additional condensational sink provided by the particle surface lowers the steady state concentration. Under conditions of unperturbed gas-phase production and typical times for phase transfer smaller than the residence time of the air in the chamber, the lowered gas-phase steady state concentrations reflect the partitioning of HOM, which is determined by the balance of condensation and evaporation. (Tröstl et al. (2016) noted that many HOM have a finite vapor pressure.) Since we are working in a steady state system, we cannot easily separate between a kinetically slow uptake and a balance between (fast) uptake in steady state with a (fast) evaporation. For molecules with finite vapor pressures steady state between condensation and evaporation is established on the time scales of less 10 minutes in our CSTR, e.g. for molecules with molecular masses of 300 Da and at a particle surface of $5.0 \times 10^{-4} \text{ m}^2 \text{ m}^{-3}$ the typical uptake time is about the same as the mixing time of 120 s. We express the net effect of condensation and evaporation by an effective uptake coefficient γ_{eff} and the gas kinetic collision rate of HOM with the particle surface. The γ_{eff} can be determined by measurement of the ratio of steady state HOM concentrations for the unseeded case and for seeded cases with the advantage that only signal intensities are required and hence no calibration is needed (Sarrafzadeh et al., 2016). In order to determine γ_{eff} we introduced seed particles into the reaction chamber by spraying ammonium sulfate solutions in two steps with concentrations of 4g/l and 40 g/L. The particles were size selected at an



electromobility diameter $d = 100$ nm. This led to bimodal size distributions in the chamber after 2 h and 3.5h with one mode around 100 nm and a second mode around 200 nm ($\approx 25\%$ by number). The diameter of the median of the surface distributions was located in arrange of 150 - 200 nm. Since it is likely that nearly every collision will lead to phase transfer of HOM, we considered the Fuchs-Sutugin correction factor (f_{FS}) to calculate the collision rate (Fuchs and Sutugin, 1971) in order to
5 correct for diffusion limitations. Taking into account the mean free path for a range of molecular compositions of $C_{10}H_{14-16}O_{4-12}$ and a median of the particle surface distribution in a range of 150-200 nm, we estimate f_{FS} in a range of 0.65-0.75; diffusivity was calculated after Fuller et al. (1969).

Briefly, $f_{FS} \cdot \gamma_{eff}$ was derived as follows. In a first step wall loss rates of HOM were measured. After stopping the OH production and thus photochemical HOM formation we observe an exponential decay of HOM signals. The exponential
10 decay of the signal intensity gives the lifetimes of those HOM. In absence of particles the lifetimes reflect the wall loss rates. As shown in Sarrafzadeh et al. (2016) and Ehn et al. (2014) the lifetimes were in the range of 70 to 150 s, i.e. the loss rates on the walls of the chamber, $L_W(HOM)$, were in the range of 1.4×10^{-3} to $7 \times 10^{-3} s^{-1}$. $L_W(HOM)$ are more than order of magnitude higher than those caused by the flush out of the air in the chamber ($3.6 \times 10^{-4} s^{-1}$ for the residence time of 46 minutes). Therefore we neglected flush out as sink for HOM.

15 In a second step, the chemical system was kept at the same steady state conditions for $[OH]_{SS}$, $[O_3]_{SS}$, and MT concentration. Increasing amounts of ammonium sulfate seed particles (electromobility diameter $d = 100$ nm) were added which instantaneously led to lowered HOM concentrations in the gas phase due to the additional loss by condensation on the seed particles.

Data evaluation was based on the following considerations: The concentration of any HOM, $c(HOM)$ is determined by its
20 production rate $P(HOM)$ and the first order loss rate, $L(HOM)$ as given in Eq. (4):

$$c(HOM) = \frac{P(HOM)}{L(HOM)} \quad (4)$$

In absence of particles the total loss rate $L(HOM)$ is given alone by the loss rate at the chamber walls, $L_W(HOM)$. In
25 presence of particles $L(HOM)$ is the sum of loss rates at the walls and at the particle surface, $L_W(HOM) + L_p(HOM)$. At constant production rate $P(HOM)$ the ratio of concentrations is inverse proportional to their ratio of loss rates:

$$\frac{c(HOM)^0}{c(HOM)} = \frac{L_W(HOM) + L_p(HOM)}{L_W(HOM)} \quad (5)$$

30 In Eq. (5), $c(HOM)^0$ is the concentration of HOM in the particle free chamber and $c(HOM)$ is the concentration in the particle containing chamber. Solving Eq. (5) for $L_p(HOM)$ we achieve Eq. (6):



$$L_P(HOM) = \frac{c(HOM)^0}{c(HOM)} \cdot L_W(HOM) - L_W(HOM) \quad (6)$$

Applying the kinetic gas theory, we achieve Eq. (7):

$$L_P(HOM) = \gamma_{eff} \cdot f_{FS} \cdot \frac{\bar{v}}{4} \cdot S_P \quad (7)$$

In Eq. (7), f_{FS} is the Fuchs-Sutugin correction, \bar{v} is the mean molecular velocity of the HOM, S_p is the surface of the particles during the respective measurement and γ_{eff} is the effective uptake coefficient. Varying $L_P(HOM)$ by varying the surface of seed particles led to a linear relationship between $L_P(HOM)$ and S_p . The coefficient γ_{eff} was obtained from the slope of such plots by dividing the values for slopes by $f_{FS} \cdot \bar{v} / 4$ with $f_{FS} = 0.7$ assuming a mean median of the surface size distribution of 175 nm.

It has to be noted γ_{eff} is only valid, if S_p is not too large for two reasons. First, in presence of a strong condensational sink, many HOM signals become close to the detection limit (here for $S_p > 1.2 \cdot 10^{-3} \text{ m}^2 \text{ m}^{-3}$). Secondly, for large $S_p (> 2 \cdot 10^{-3} \text{ m}^2 \text{ m}^{-3})$ distinct deviations from linearity were observed, likely due to fact that the time scales of losses of peroxy radicals on particles become similar to the time scales of peroxy radical reactions (Pullinen, 2017). If so, the production rates $P(HOM)$ of HOM termination products are not constant but decrease significantly with increasing particle load.

3 Results

3.1 Yields of organic nitrates from β -pinene photo-oxidation

In the first step we determined the potential of organic nitrate (ON) formation in a β -pinene / NO_x mixture ($[\beta\text{-pinene}]_0 \sim 39$ ppb / $[\text{NO}_x]_0 \sim 50$ ppb). The β -pinene and NO_x were added to the chamber that contained about 60 ppb O_3 . The OH production was started by switching on the UV lamp (time = -2.4h in Figure 1), inducing the photochemical oxidation of β -pinene and thereby the ON production. As shown in Figure 1, concentrations of β -pinene and NO_x decreased in the presence of OH. When the photochemical system was in a steady state after about two hours (time $t = 0$ h in Figure 1) the β -pinene addition was stopped and β -pinene concentration decreased to zero. In parallel, [OH] increased leading to a lower NO_x concentration. At time $t = 1.7$ h, the OH concentration was re-adjusted to the same OH level as before the removal of β -pinene by lowering $J(\text{O}^1\text{D})$. The decrease in [OH] caused an increase of $[\text{NO}_x]$ by 15 ppb to 32 ppb. Considering the NO_x level of 20 ppb before the β -pinene had been removed, the net NO_x increase amounts to 12 ppb. The inflow of NO_x as well as the OH concentration were the same before and after removal of β -pinene, but now $[\text{NO}_x]_{ss}$ was higher. Hence, with β -pinene we removed a strong NO_x sink in the chamber. Most of this NO_x sink is made up by reactions of NO and NO_2 with peroxy radicals and peroxy acyl radicals that lead to ON formation (reactions R5 and R6). Thus, the difference in $[\text{NO}_x]_{ss}$ in presence and in absence of β -pinene allowed to calculate the fraction of ON formed from β -pinene. Defining the yield of ON



formation as the molar amount of NO_x “released” by not forming β -pinene ON over the molar amount of consumed β -pinene and with the assumption that one lost NO_x molecule had produced one ON molecule we derived a molar yield of ~36% for the ON formed from β -pinene. For later comparison with AMS results we calculated the mass concentration of nitrate bound to the organic moieties (OrgNO_3), again with the assumption that one lost NO_x molecule produces one OrgNO_3 . A total
5 mass concentration of $33 \mu\text{g m}^{-3}$ OrgNO_3 in the gas phase was obtained at the given condition in the chamber. The mass concentration of HNO_3 formed during this time was about $24 \mu\text{g m}^{-3}$ (for details of these calculations see supplement section S3).

3.2 HOM formation from α -pinene- and β -pinene photo-oxidation

We observed multifunctional peroxy radicals (HOM-RO_2) as well as their termination products in the high resolution mass
10 spectra. The latter are formed in accordance with established pathways of peroxy radical chemistry (Bianchi et al., 2019). We will distinguish HOM-PP, which arise from permutation reactions of HOM-RO_2 with peroxy radicals including HO_2 , and HOM-ON, which are formed in reaction of HOM peroxy and HOM acyl peroxy radicals with NO or NO_2 . In addition we found HOM accretion product with $\text{C}_{>10}$ and $\text{C}_{<20}$ (HOM-ACC).

We observed two major differences in HOM formation and product patterns for α -pinene and β -pinene:

15

1. For α -pinene with an endocyclic double bond, a certain fraction of the HOM was produced by ozone reactions whereas ozonolysis of β -pinene, with an exocyclic bond, did not produce significant amounts of HOM.
2. The HOM products of α -pinene in the monomer region mainly consisted of C_{10} -molecules. In β -pinene fragmentation during the oxidation process is stronger and we observed progressions of C_{10} , C_9 , C_8 , and C_7 HOM.
20 This led to overlapping peaks in the mass spectra. E.g. molecular masses where 1 C-atom and 4 H-atoms are replaced by 1 O-atom were not fully resolved. However, by peak fitting we were able to attribute the contributing formula components in most cases (see supplement section S2 and peak list in supplement section S6). In addition, fragmented peroxy radicals in β -pinene form a larger variety of accretion products with less than 20 C-atoms.

25 Besides these differences, the behavior with respect to NO_x addition was very similar for α -pinene and β -pinene photo-oxidation: increase of HOM-ON (increase of peaks with odd molecular masses odd peaks), decrease of accretion products and a shift of HOM monomers to the higher m/z .

3.3 Decrease of accretion products

With increasing NO_x we observed a strong decrease of HOM-ACC at $m/z > 420$ Th relative to HOM monomers at $m/z < 340$
30 Th. These can be clearly seen in the HOM mass spectra obtained for α -pinene and β -pinene in Figure 2. To quantify the effect, the mixing ratio of HOM-ACC products (i.e. compounds C_n with $n > 10$ for $m/z > 420$ Th) were summed up and normalized as described in supplement section S3. Figure 3 shows the decrease of the mixing ratio of the HOM-ACC with



NO_x. At low NO_x conditions, those accretion products contributed to 35 % - 40 % and monomers (i.e. compounds C_n with n ≤ 10 for m/z < 340 Th) contributed between 60 % and 65 % to the total concentration of HOM. At the highest NO_x level the concentration of HOM-ACC was suppressed by about 95%. In comparison, the sum of HOM-PP (molecular mass range 230 – 340 Da) is diminished only by less than 40 %. The decrease of HOM-ACC mixing ratio is attributed to the competition
5 between HOM-ON formation channels (R5 and R6) and HOM-ACC formation channel (R4a): in presence of NO_x more HOM-ON monomers were formed and less HOM accretion products.

3.4 Detection of termination permutation products of peroxy radical - peroxy radical reactions and HOM-organic nitrates

At low NO_x conditions, HOM-PP with even molecular masses showed the highest concentrations. HOM-ACC are also
10 produced from peroxy-peroxy permutation reactions, but their intensity decreased strongly and HOM-ACC are barely observed at high NO_x condition, as described in previous section 3.3. For that reason, we focus on monomer products in the following considerations in section 3.5-3.7.

Because of the complexity of the product spectrum the character of the functional group formed in the termination step of HOM-PP cannot be derived unambiguously from the available elementary molecular formulas alone. As an example, HOM-
15 PP with the molecular formula C₁₀H₁₆O_x can be hydroperoxides formed from peroxy radicals with molecular formula C₁₀H₁₅O_x in reaction R3, they can be alcohols formed from peroxy radicals C₁₀H₁₅O_{x+1} in reaction R4, or they can be ketones formed from peroxy radicals with the molecular formula C₁₀H₁₇O_{x+1} in reaction R4. Dependent on the specific precursor peroxy radical, they can also be carboxylic acids or percarboxylic acids. We therefore lump the monomer HOM with even masses (HOM-PP) together independent of the chemical character of the termination group. In case of β-pinene, we did
20 not separate the contributions from different progressions (e.g. C₁₀H_YO_x and C₉H_{Y-4}O_{x+1}) but used the overall signal under the peak for further analysis and indicate the main components under the peak (e.g. Figure. 5). Separation between HOM-PP and HOM-ON was easier, because HOM-ON have odd molecular masses. Peroxy radicals (without N) also contribute to the odd mass peaks, but in most cases they could be separated by the mass defect. Other contributors to odd mass peaks are HOM containing ¹³C and clusters with the nitrate dimer (HNO₃NO₃⁻) of HOM-PP, but the latter contribution was small
25 (supplement section S2). Analysis of the high resolution mass spectra for α-pinene revealed that HOM-ON-peroxy radicals are rare. Peak lists for the HOM measured in the absence and presence of NO_x are given in the supplement section S6. (Note that we cannot *a priori* distinguish between HOM-ON formed in reactions R5 and R6, respectively).

Figure 4 demonstrates the change in the HOM pattern when NO_x is added to the reaction system. At low NO_x levels, HOM- PP (black) were predominant, but already at the medium NO_x levels the concentrations of HOM-ON (blue) were similar to
30 HOM-PP (black). HOM-ON concentrations increased on the cost of HOM-PP. The product spectra of β-pinene showed a similar shift from HOM-PP to HOM-ON.

With increasing NO_x we observed a small but increasing fraction of highly oxidized nitrates with C < 10. Their chemical formulas have low H:C ratio compared to gas-phase C₁₀ HOM-ON. Supposedly, they did not arise from gas-phase chemistry



but were formed at the walls. Their time series was not responding to the changes of experimental conditions like start of photochemistry or cease of NO_x addition, instead these compounds increased steadily after NO_x addition. For α -pinene, their maximum contribution appeared at 74 ppb $\text{NO}_{x,ss}$ where they mounted up to 8% of the total HOM concentration and 17% of the HOM-ON concentration. Below 35 ppb NO_x their contribution was less than 7% and 12%, respectively. For β -pinene, this was less distinct and the contribution was only 2 to 3 %. Because these HOM-ON had $C < 10$ and appear at the lower end of the mass spectrum, their contribution to HOM mass (and therewith SOA mass) were small, and we did not correct for these products.

3.5 Effective uptake coefficients for HOM-PP and HOM-ON.

Based on identified HOM-ON and HOM-PP, we characterized their potential contribution to SOA formation by determining their loss rates on particles $L_p(\text{HOM})$, Eq.6. According to Eq.7, plots of $L_p(\text{HOM})$ versus particle surface, S_p , should exhibit a linear dependence between $L_p(\text{HOM})$ and S_p allowing determining effective uptake coefficients, γ_{eff} . However, for conditions with sufficient HOM production, we could not suppress all new particle formation. As a result $c(\text{HOM})^0$ in Eq.5 and 6 had to be extrapolated in order to separate loss to particle $L_p(\text{HOM})$ and loss to the walls $L_w(\text{HOM})$. With $c(\text{HOM})^0$ $L_p(\text{HOM})$ is calculated and by Eq. (7) γ_{eff} can be derived by applying $f_{\text{FS}} = 0.7$ to the slope of $L_p(\text{HOM})$ as a function particle surface S_p (Figure 5). Figure 5 is based on HR data, which show substantial scatter. In order to reduce the error we used the respective unit mass resolution (UMR) data, which on general showed better signal to noise than the individual HR peaks under the same UMR signal.

In Figure 6 we compare γ_{eff} for HOM with the same number of O-atoms. Note that compared to their chemical sum formula, ON were shifted by one O to lower O in order to account for the addition of NO. When comparing data for HOM with the same numbers of O-atoms (in the precursor peroxy moiety), no significant and systematic differences were found for γ_{eff} within the uncertainty limits, i.e. the potential to condense on particles was about the same for HOM-PP and HOM-ON. For HOM moieties with 8 and more O-atoms, γ_{eff} approaches 1 independent if they were HOM-PP or HOM-ON. HOM-PP and HOM-ON with 6 and more O-atoms with upper limits of γ_{eff} near 0.5 will still reside to a large portion in the particle phase therefore they should contribute to SOA mass.

3.6 Organic bound nitrate in SOA and in gas-phase HOM-ON

SOA yields for α -pinene and β -pinene (wall loss corrected) were between 0.08 and 0.18, thus in the same range as those reported by Sarrafzadeh et al. (2016). SOA mass formed and the SOA yields changed with addition of NO_x to the photochemical system because NO_x affects $[\text{OH}]_{\text{SS}}$ and thereby also the formation of higher generation products. The mass fractions of OrgNO_3 in the SOA particles are shown in Figure 7. They were calculated for the different NO_x concentrations by dividing the mass concentration of OrgNO_3 by the mass concentration of the respective organic as measured with the AMS. The fraction of OrgNO_3 in particles was dependent on the NO_x concentrations. It was negligible when no NO_x was added and increased steadily with increasing $[\text{NO}_x]$. At the same time, also the fraction of inorganic nitrate increased with



increasing $[\text{NO}_x]$, but was a factor of about 3 lower than that of OrgNO_3 (Figure 7). While $\sim 24 \mu\text{g m}^{-3}$ HNO_3 were formed in the gas phase, less than $0.1 \mu\text{g m}^{-3}$ of inorganic nitrate was found in the particle phase. For the same $[\text{NO}_x]$, the mass fractions of organic or inorganic nitrate in SOA were about the same for α -pinene and β -pinene, indicating that the formation of condensable OrgNO_3 was similar. The determination of OrgNO_3 comprises some uncertainty, but even if we count all
5 inorganic nitrate as OrgNO_3 we get an upper limit of less than 4%.

We compared the amount of OrgNO_3 in particles to that in the gas phase. As shown in section 3.1, at $[\text{NO}_x]_{\text{SS}} \sim 20$ ppb about $33 \mu\text{g m}^{-3}$ OrgNO_3 was formed in the gas phase. At similar $[\text{NO}_x]_{\text{SS}}$ and similar β -pinene concentrations ($[\text{NO}_x]_{\text{SS}} \sim 22$ ppb, $[\beta\text{-pinene}]_{\text{SS}} \sim 6$ ppb) the fraction of OrgNO_3 in the particle phase was only $1.6 \pm 0.64\%$ (Fig. 7), i.e. less than $0.4 \mu\text{g m}^{-3}$ OrgNO_3 was bound in particles. We conclude that many ON are too volatile to significantly contribute to the particulate
10 phase. However, considering the low volatility HOM-ON (section 3.5), HON-ON should contribute to particle mass eventually providing the particulate OrgNO_3 . We estimated the mass fraction of OrgNO_3 bound in HOM-ON. For this we considered all HOM with 6 and more O-atoms in the HOM-moiety because their γ_{eff} is large enough to partition significantly into the particle phase and to contribute efficiently to SOA mass. As shown in Figure 6, the HOM partitioned without preference, independent of being HOM-PP or HOM-ON. We first determined the fraction on a molecular base by
15 using the ratios of signal intensities, which is identical to using concentrations c :

$$\frac{c(\text{HOM-ON})}{c(\text{all HOM})} \approx \frac{\sum_{241}^{405} c(\text{HOM-ON})}{\sum_{230}^{550} c(\text{allHOM})} \quad (8)$$

In Eq.8, the left hand term represents the molar fraction of HOM-ON. We summed all HOM with $\text{O} \geq 6$, which included all
20 HOM with $\gamma_{\text{eff}} > 0.5$ and provides a lower limit. Signals at $m/z > 550$ Da were not taken into account, since they were very low at high NO_x levels and thus uncertain. In a second step we calculated from Eq.8 the mass ratio of OrgNO_3 . We split all HOM in the denominator of Eq.8 in HOM-ON and other termination products and multiplied the concentrations with the respective molar weight (Eq.9). The numerator was multiplied with the molecular weight of the nitrate termination group:

$$25 \frac{M(\text{OrgNO}_3)}{M(\text{organic})} \approx \frac{\sum_{241}^{405} c(\text{HOM-ON}) \cdot 62}{\sum_{230}^{550} c(\text{other term.prod.}) \cdot m + \sum_{241}^{405} c(\text{HOM-ON}) \cdot (m-62)} \quad (9)$$

In words, the left hand term in in Eq.9 gives the ratio of the total mass of OrgNO_3 over the total organic mass of HOM with $\gamma_{\text{eff}} > 0.5$ ($\text{O} \geq 6$). This value can be compared with the direct AMS observation of OrgNO_3 . Figure 8 shows the molecular ratios (calculated by Eq.8) and the mass fractions (Eq.9) in dependence on NO_x . For α -pinene we were able to
30 separate HOM-ON and HOM-RO₂ unambiguously (see supplement). For β -pinene we give lower and upper limits of the molecular and mass fractions, because of uncertainties in the HR analysis that were induced by the stronger fragmentation and overlapping progressions of compounds with different number of C but same unit molecular mass. For the lower limit shown in Figure 8, we applied a peak list with all identified signals at low and high NO_x concentrations for fitting, whereas



the upper limit was achieved by using the peak list optimized for high NO_x cases. (The reason for the spread can be explained as follows: the approach with the peak list with all identified peaks attributes some HOM-RO₂ to the HOM-ON signal, independent if the specific HOM-RO₂ exist in the chemical system or not, while the approach with the high NO_x peak list has the tendency to falsely attribute HOM-ON to existing HOM-RO₂ missing in the high NO_x peak list.)

5 Both, HOM-ON and OrgNO₃ mass fraction increased with $[\text{NO}_x]$, similarly for both MT. For α -pinene about 40 % of the detected HOM were HOM-ON and more than 10 % of the HOM mass was OrgNO₃ once $[\text{NO}_x]$ was larger than 30 ppb ($[\text{BVOC}]_{\text{SS}}/[\text{NO}_x]_{\text{SS}} < 2$ ppbC/ppb). For upper limit case of β -pinene we achieved about the same fractions as observed for α -pinene (50 ppb NO_x : $[\text{BVOC}]_{\text{SS}}/[\text{NO}_x]_{\text{SS}} < 1.1$ ppbC/ppb). Since we considered only HOM that efficiently condense on particles, one would expect that OrgNO₃ brought by HOM-ON alone should contribute about 10 % of the SOA mass. This
10 was not the case, as the direct comparison in Figure 8 shows. The maximum contribution of particulate OrgNO₃ was about 3 %, i.e. the measured OrgNO₃ was a factor of 3 to 4 lower than expected: the OrgNO₃ bound in low volatility HOM-ON which could potentially contribute to SOA mass was significantly higher than OrgNO₃ directly observed in the particle phase.

15 3.7 Mass concentration of HOM

To estimate an possible effect of hydrolysis of OrgNO₃ and re-evaporation of HNO₃, potential condensable mass concentration (c^{Mass}) was derived by weighing the concentration (c_i^N) of each HOM_{*i*} by its molecular mass (M_i) in the range of 230 Da to 550 Da:

$$c^{\text{mass}} = \sum_{230}^{550} c_i^N \cdot M_i$$

20

Herein c^N is the concentration was that was corrected according to the method described in supplement section S2. Figure 9 shows the calculated mass concentrations with and without hydrolysis in dependence on NO_x . The relative uncertainty limits were estimated to 19%. The uncertainty was estimated from the standard deviation of the data obtained at low $[\text{NO}_x]$ conditions (9 measurements). Uncertainties of $[\text{NO}_x]_{\text{SS}}$ were estimated to $\pm 10\%$. The uncertainty of absolute
25 concentrations caused by the uncertainty of the calibration factor (see supplement S1) is much higher than the uncertainty limits shown in the Figure 9. However, as the systematic error of the calibration factor is the same for each data point it does not affect the observed trend of only somewhat decreasing mass concentrations of HOM with increasing NO_x .

In case of HOM-ON, c^{mass} includes the mass of OrgNO₃. According to Bean and Hildebrandt Ruiz (2016), hydrolysis of OrgNO₃ and evaporation of HNO₃ from condensed HOM-ON can cause mass loss by about 20%. We indicate the resulting
30 SOA mass after considering OrgNO₃ loss by hydrolysis by a prime as $c^{\text{mass}'}$ in Figure 9 (details for the calculations of $c^{\text{mass}'}$



see section 4.3).

It is obvious from Figure 9 that the mass concentration of condensable HOM is about 30% lower at the highest NO_x conditions compared to those at low NO_x conditions. It is furthermore evident that the differences between c^{mass} and $c^{mass'}$ are quite low which is showing re-evaporation of HNO_3 is of minor importance for explaining the SOA mass suppression with increasing NO_x in the system. An explanation must then be the observed strong decrease of the accretion products with increasing NO_x as shown in Figure 2.

4 Discussion

4.1 Organic nitrates and SOA formation.

Several studies on organic nitrates or organic bound nitrate in SOA refer to reactions of unsaturated volatile organic compounds with NO_3 (Fry et al., 2013, 2014; Kiendler-Scharr et al., 2016; Lee et al., 2016a, Faxon et al., 2018). The pathway of forming ON by NO_3 was negligible in our experiments as we applied quite high light intensity, humidity and also high NO concentrations during our experiments. These experimental conditions inhibited formation of NO_3 at relevant concentrations because NO_3 was efficiently destroyed by photolysis, by reactions with NO and by scavenging of N_2O_5 at the humid surfaces of the chamber walls. The HOM-ON measured during our experiments were formed in reactions R5 and R6.

There are some studies with respect to the SOA content of ON formed by photo-oxidation (Nozière et al., 1999; Rollins et al., 2010; Xu et al., 2015b; Berkemeier et al., 2016; Lee et al., 2016b; Zhao et al., 2018) wherein in most cases only the mass fraction of ON of the total SOA mass is reported. To convert reported mass fraction of ON to the mass fraction of OrgNO_3 we use the factor 1/5 which assumes an average molar weight of ON of about 309 Da as derived from our observations of HOM-ON with $\gamma_{\text{eff}} > 0.5$ (see supplement, section S6).

According to literature data, ON produced during photo-oxidation or ozonolysis contribute between 3 % (Lee et al., 2016b) and 40% (Berkemeier et al., 2016) to the total SOA mass. Using a conversion factor of 1/5 means that OrgNO_3 should contribute between 0.6 % and 8 % to the total SOA mass. We found contributions between 0 % and 2.7 % by AMS, which is within the range of most other data reported in the literature but at the lower end. We showed that the contributions of OrgNO_3 depend on the NO_x level ($[\text{VOC}]/[\text{NO}_x]$ level) as expected from established peroxy radical chemistry in presence of NO_x . This finding can probably explain the wide range of ON fractions reported in SOA formation. Detailed and meaningful comparison of our data to those reported in literature requires knowing the $[\text{VOC}] / [\text{NO}_x]$ ratios during SOA formation in the respective experiments. The VOC to NO_x ratio is known for other experiments made by us in the SAPHIR chamber in Jülich (Zhao et al., 2018). Zhao et al. (2018) achieved a mass fraction of 11% for OrgNO_3 which is much higher than the mass fractions we found. Interestingly, the 11% found by Zhao et al. (2018) are close to $M(\text{OrgNO}_3)/M(\text{Organic})$ determined for the HOM-ON themselves in this study. These findings will be further discussed in section 4.3.



4.2 Effective uptake coefficients

We provided data on effective uptake coefficients, γ_{eff} , which allowed differentiation between SVOC, LVOC and ELVOC. The dependence of γ_{eff} on the number of O-atoms in the HOM (Figure 6) suggests that the OrgNO₃ found in SOA predominantly originates from HOM-ON with 6 and more O-atoms. We conclude that less oxidized ON with few O-atoms are not so important for the formation of SOA mass at least at small loads of SOA. This conclusion is confirmed by our observation of low amounts of OrgNO₃ in HOM-ON and in the particle phase despite of large molecular yields (> 30%, section 3.1) of OrgNO₃ produced in the gas phase. From all ON only a few percent - the HOM-ON - made it into the particulate phase (sections 3.1 and 3.6).

Our findings are in agreement with observations by Lee et al. (2016b) in a field study. They found HOM-ON in the gas phase as well as in the particle phase and show that the distribution of signal intensities for HOM-ON in the gas phase is different from that in the particle phase. Comparing the signal intensities for HOM-ON with the same number of O-atoms between gas phase and particle phase, respectively (Figure 2 in Lee et al., 2016b), it seems that the higher the number of O-atoms, the more the ON partition in the particle phase. As there was no calibration for gas phase HOM-ON, absolute numbers for partitioning coefficients or effective uptake coefficients were not obtained. Our data are qualitatively consistent with those of Lee et al. (2016b), suggesting that the basics of HOM-ON condensation in our laboratory studies are similar to those in the environment.

Comparison between γ_{eff} determined for HOM-PP and HOM-ON indicated that there were no significant and systematic differences at least for the HOM moieties with more than 6 O-atoms. This can be understood from the basics of group contribution models (Capouet and Müller, 2006; Pankow and Asher, 2008): HOM peroxy radicals with more than 6 O-atoms already carry protic functional groups - OH, -OOH, C(=O)OH, or C(=O)OOH - from the several autoxidation steps. Thus their vapor pressure is low because of the ability to form (multiple) hydrogen bonds. The termination reactions R3, R4, R5, and R6 only form one more functional group of the respective HOM. Except of the functional group added by the termination reaction, distributions of functional groups are the same for all monomer termination products originating from the same HOM peroxy radical. This also includes HOM-ON. Hence, no substantial differences should be expected for the vapor pressures of all monomer termination products produced originating from the same HOM peroxy radical.

Considering the molecular mass instead of O-atoms of the HOM moiety, HOM-ON have higher vapor pressure compared to HOM-PP (Peräkylä et al., 2019), despite of the heavier termination group -ONO₂ compared to -OOH, =O, or -OH. Note, that the number of functional groups cannot be inferred one to one from the number of O-atoms. HOM-peroxy radicals can be formed via autoxidation of peroxy radicals or via H-shifts and O₂ addition in alkoxy radicals and thus there may be different numbers of O-atoms per functional groups. In addition, peroxy radicals may have the same molar weights but may have different molecular structures. With this limitation in mind, we will exploit the relationship between γ_{eff} and O atoms as proxy for the number of functional groups in the next step of interpretation.



Starting from a given HOM-peroxy radical, the number of functional groups in the termination products is the same, independent if a HOM-PP or a HOM-ON is being formed. However, the masses of HOM-PP and HOM-ON differ. If a HOM-ON is formed, it contains 1 N and 1 or 2 O-atoms more than the parent HOM peroxy radical (depending on NO or NO₂ being added). If a HOM-PP is formed in a reaction of the same HOM peroxy radical with another peroxy radical, the number of O-atoms stays constant and in case of ketone or alcohol formation, the number of O atoms decreases by 1. This means that the formation of HOM-ON generally increases the molecular mass compared to a HOM-PP (and this was considered in Figure 6). Since the γ_{eff} are similar for all monomer HOM originating from the same HOM peroxy radical, i.e. HOM-PP and HOM-ON have similar vapor pressures, a gain of SOA mass should be expected if HOM-ON are produced instead of HOM-PP (10% for NO and a molar weight 309). However, whether this potential mass gain is realized in a long term net increase of SOA mass in NO_x containing systems will depend on the fate of the ON in the particle phase.

4.3 Comparison of OrgNO₃ in HOM to OrgNO₃ in particles

Comparing the data shown in Figure 8, it is obvious that the fraction of OrgNO₃ in the gas-phase HOM-ON is 3 to 4 times higher than that found in the particulate phase. As all considered HOM (Eq.8 and 9) have a high efficiency for particle mass formation, a fraction of about 10 % OrgNO₃ would be expected in the particle phase. Of course there are uncertainties; but, applying the same instrumentation and using the same evaluation schemes as here, Zhao et al. (2018) find a fraction of 11% for OrgNO₃, i.e. mass closure as expected if all HOM with more than 6 O-atoms contribute to SOA formation. A difference between the experiments here in JPAC and Zhao et al. (2018) in SAPHIR was the relative humidity which was about 30 % by Zhao et al. (2018) and 63% in the study here. We suggest that the RH may be the key to bring this study and the results by Zhao et al. (2018) in agreement, although we cannot provide further experimental proof. However, there are several studies implying that ON undergo hydrolysis in the condensed phase (Day et al., 2010; Liu et al., 2012; Browne et al., 2013; Jacobs et al., 2014; Rindelaub et al., 2016, 2015; Boyd et al., 2015; Bean and Hildebrandt Ruiz, 2016; Lee et al., 2016b). Thus, hydrolysis can be suspected as a mechanism explaining both, the lower fraction of OrgNO₃ in the particle phase compared to that stored in HOM organic nitrates and the lower amount of OrgNO₃ found in this study compared to that found by Zhao et al. (2018).

In addition, hydrolysis of OrgNO₃ could contribute to SOA mass suppression. We estimated the effect of ON hydrolysis on the remaining SOA mass under the assumption that all HOM-ON with $\gamma_{\text{eff}} > 0.5$ had condensed on SOA. By hydrolysis of organic nitrates HNO₃ is formed and the nitrate functionality at the organic rest is replaced by an OH group. HNO₃ is too volatile to stay in the particle phase (e.g., Browne et al., 2013; Romer et al., 2016) and we found only negligibly small amounts of inorganic nitrate in particles despite of high HNO₃ production in the gas phase (section 3.1). As a consequence, on average 1/5 of the mass of the HOM-ON that originally condensed on particles might re-evaporate and indeed reduce the amount of condensed mass. The question is what happens to the remaining organic moiety. As long as hydrolysis does not lead to fragmentation of the organic rest, hydrolysis just replaces the nitrate group by the protic OH group. The number of



functional groups remains the same and no strong changes in the vapor pressures are expected for the organic rest. As a consequence the organic rest of the former organic nitrate would stay in the particle phase. If so, hydrolysis and re-evaporation of HNO_3 should not lead to a mass loss high enough to explain the often observed suppressing effect of NO_x on SOA mass formation in laboratory studies. The mass loss per evaporated HNO_3 is 63 Da. The water molecule driving the hydrolysis can be from gas-phase or particulate phase and exchange of water between the phases is fast. The de facto mass loss therefore should be 45 Da per evaporating HNO_3 . A part of this loss is “compensated”; depending on the HOM-ON being formed by NO or NO_2 and, depending on the HOM-PP not produced instead of the organic nitrate, this mass gain is between 29 Da and 63 Da per formed HOM-ON. Thus, the net effect of mass gain by the formation of a HOM-ON instead of a HOM-PP in the gas phase and the possible mass loss due to evaporation of HNO_3 from the particle phase should be very low or negligible.

10 4.4 Suppression of accretion products and SOA yield

In the previous section we have shown that the formation of organic nitrates instead of other HOM monomer termination products cannot explain the suppressing effect of NO_x even if we consider hydrolysis and loss of HNO_3 . The most probable explanation for the NO_x induced suppression of SOA formation in laboratory studies is the suppression of HOM-ACC formation. At low NO_x conditions, the mixing ratio of HOM-ACC is similar to those of monomers. Considering that HOM with masses below 230 Da do not effectively contribute to particle formation and the fact that the average mass of HOM-ACC is much higher than the average mass of monomers, it is clear that the contribution of HOM-ACC to SOA mass formation can be even higher than the contribution of monomers. Hence, suppression of HOM-ACC formation by NO_x might lead to a strong suppression of particle mass formation.

The precursors of the respective HOM-ACC are the key to understand whether the suppression of HOM-ACC formation lead to a suppression of SOA mass. We therefore now analyze the mass change if HOM-ACC are formed instead of monomer termination products. According to reaction R4a, HOM accretion products are produced from two peroxy radicals (Berndt et al., 2018a, 2018b). The other product of this reaction is molecular oxygen and thus the molecular mass of the HOM accretion product is lower by 32 Da than the sum of the masses of both monomer peroxy radicals. If two organic nitrates are formed from these peroxy radicals instead of the HOM-ACC, each of them gains mass due to the addition of NO or NO_2 (reactions R5 and R6). Comparing the molecular mass of the HOM-ACC with that of two organic nitrates formed from the same peroxy radicals, there may be a mass gain of 92 Da to 124 Da when two HOM-ON are formed instead of one HOM-ACC. This gain comprises addition of two NO or two NO_2 and the O_2 loss in the HOM-ACC formation process. Hence, if the respective HOM-ACC is formed by HOM peroxy radicals that anyhow would form low volatility termination products, the loss of HOM accretion products, and instead generating two HOM monomers at the same time, should lead to an increase of total condensable mass.

The situation is different if we assume that peroxy radicals with lower O:C ratio are involved in the HOM-ACC formation besides a HOM peroxy radical. In this case, the volatility of its monomeric termination products may be too high to allow



effective condensation. In such cases, HOM-ACC formation can indeed lead to a net gain of condensable mass: nearly the whole molecular mass of the “non SOA forming” peroxy radical is converted to condensable mass (except of the O₂ lost in reaction R4a). In other words, suppression of accretion product formation would lead to mass loss via “non SOA forming” peroxy radicals (compare accretion product suppression by isoprene peroxy radicals, McFiggans et al., 2019).

5 Mass loss can be even stronger when two intermediate level oxidized (functionalized) peroxy radicals are involved in the accretion product formation. In this case, the loss can be nearly as high as the whole mass of the accretion product. Such effect can be verified by the average O:C ratio derived from high resolution peak identification. For α -pinene at the background level of NO_x the average O:C is 0.97 for the monomers and 0.68 for the accretion products. The lower O:C ratios of HOM-ACC indicate a substantial contribution of peroxy-radicals with low numbers of O atoms. HOM-ACC can be formed from
10 many combinations of precursor peroxy-radicals and therefore, clear identification of the respective precursors is not possible.

Referring to rate coefficients reported by Berndt et al. (2018b), which decrease with the degree of functionalization by two orders of magnitude, we speculate that there are three types of pathways to accretion products: HOM-RO₂· + HOM-RO₂·, HOM-RO₂· + RO₂·, and RO₂· + RO₂· (for HOM-RO₂· + RO₂· accretion products of cyclopentene compare Mentel et al.,
15 2015). For illustration we simply assume that accretion product formation involves a pre-stabilized adduct (in analogy to the Lindemann-Hinshelwood mechanism). Then HOM-RO₂· + HOM-RO₂· would form a relatively long lived and relatively stable adduct because of the high functionalization of the reactants (with protic functional groups). Such adduct would have enough time to react to the accretion products e.g. as proposed by Valiev et al. (Chem. Comm., 2019). HOM-RO₂·+RO₂· form weaker adducts with shorter lifetimes, but there are more collisions to form adducts as [RO₂·] are higher than [HOM-RO₂·]. RO₂· + RO₂· may still take place, driven by bare number of collisions. All involved RO₂· must have certain degree
20 of functionalization. First generation RO₂· contain only 3 O-atoms, but are by far the most abundant. Reactions of first generation peroxy radicals could therefore still make a contribution to accretion products.

We conclude that suppression of HOM accretion product formation is a mechanism that leads to lower amounts of condensable mass because of involvement of non SOA forming RO₂· and therefore can explain the suppressing effect of
25 NO_x on SOA mass formation. Note that in the experiments here RO₂· dominates over HO₂·. This is often the case in laboratory studies with enhanced VOC and oxidant levels. Insofar, suppression of accretion products may well explain the NO_x dependence (and the variability) observed in laboratory studies. In the atmosphere, photochemical accretion product formation at low NO_x is often less important because termination reactions with HO₂ are more important for HOM formation than termination reactions with RO₂ (compare Berndt et al., 2018a for example of isoprene).

30 5 Summary and conclusion

We characterized the role of ON for SOA mass formation. One finding was that low functionalized ON do not contribute much to particle formation. Only HOM-ON with more than 6 O-atoms at the HOM moiety can efficiently contribute to SOA



mass formation at least at mass loads as investigated here. Thereby HOM-ON with 6 to 7 O atoms showed partitioning with γ_{eff} of about 0.5, i.e. about 50% staying in the particulate phase. Once the HOM-ON contained more than 8 O-atoms their loss on particles was collision limited and nearly 100% resided in the particulate phase. This supports expectations that HOM-ON with more than 8 O-atoms will have extreme low volatility. No significant and systematic differences in γ_{eff} were found between HOM-ON and HOM-PP when they have the same number of O-atoms in the moiety, i.e. when they arise from the same HOM-RO₂. Hence, different volatility of HOM-ON and HOM-PP from different termination reactions can be discarded as reason for the suppressing effect of NO_x on SOA mass formation. Hydrolysis of HOM-ON in the particle phase and re-evaporation of HNO₃ seems also insufficient to explain the suppressing impacts of NO_x on SOA mass formation. Re-evaporation of HNO₃ more or less just compensates the mass gain due to the formation of a HOM-ON instead of a HOM-PP. Thus we conclude that formation of HOM-ON instead of HOM-PP (i.e. hydroperoxides, -alcohols, -ketones, -carboxylic or -percarboxylic acids) cannot be the main reason for the often observed suppressing effect of NO_x on SOA formation in photochemical systems. Since a suppressing effect of NO_x on SOA mass formation is well documented in the literature, there must be other mechanisms causing this suppression. We have observed strong suppression of HOM-ACC with increasing [NO_x]. Formation of HOM-ON via fast R5 in competition to R4a is probably the reason of the observed phenomenon, especially if R5 prevents that less functionalized RO₂ are trapped in low volatility accretion products. Without forming accretion product, there is no chance for them to participate in SOA mass formation because of the high volatility of their other termination products. Keeping off less functionalized HOM-RO₂ from forming accretion products leads to loss of one molecular mass unit of less functionalized RO₂ or even the whole accretion product if it was formed by two intermediate level oxidized peroxy radical. There is another contribution left for an explanation of SOA mass suppression by NO_x: the decomposition of alkoxy radicals that are formed in reaction R4. At the current stage this is difficult to address and needs closer study (in preparation).

Data availability

All data given in figures can be displayed in tables or in digital form. This includes the data given in the Supplement where we describe. Please send all requests for data to t.mentel@fz-juelich.de.

Author contributions

TFM, JW, EK, IP, AW, and AKS designed the experiments. Instrument deployment and operation were carried



out by IP, SS, MS, PS, SA, EK, FR, MS, RT, JW, CW, and DZ. Data analysis was done by IP, SK, SS, FR, PS, and RT. IP, SK, SS, JW and TFM interpreted the compiled data set. IP, SK, JW, TFM, and AKS wrote the paper. All co-authors discussed the results and commented on the paper.

Competing interests

- 5 Sebastian Schmitt works for TSI GmbH. The authors declare that they have no conflict of interest.

Acknowledgements

This work was supported by the European Commission's 7th Framework Program under grant agreement no. 287382 (Marie Curie Training Network PIMMS).

10

References

- 15 Atkinson, R.: Gas-Phase Tropospheric Chemistry of Organic Compounds, J. Phys. Chem. Ref. Data, Monograph No. 2, 1994.
- Atkinson, R.: Gas-Phase Tropospheric Chemistry of Volatile Organic Compounds: 1. Alkanes and Alkenes, J. Phys. Chem. Ref. Data, Vol. 26, No. 2, 215-290, doi: 10.1063/1.556012, 1997.
- Bean, J. K., and Hildebrandt Ruiz, L.: Gas-particle partitioning and hydrolysis of organic nitrates formed from the oxidation of α -pinene in environmental chamber experiments, Atmos. Chem. Phys., 16, 2175-2016, doi:10.5194/acp-16-2175-2016, 2016.
- 20 Berkemeier, T., Ammann, M., Mentel, T. F., Poschl, U. and Shiraiwa, M.: Organic nitrate contribution to new particle formation and growth in secondary organic aerosols from α -pinene ozonolysis, Environ. Sci. Technol., 50, 6334-6342, doi: 10.1021/acs.est.6b00961, 2016.
- 25 Berndt, T., Richters, S., Jokinen, T., Hyttinen, N., Kurten, T., Otkjaer, R. V., Kjaergaard, H. G., Stratmann, F., Herrmann, H., Sipila, M., Kulmala, M., and Ehn, M.: Hydroxyl radical-induced formation of highly oxidized organic compounds, Nat. Comm., 7, 10.1038/ncomms13677, 2016.
- Berndt, T., Mentler, B., Scholz, W., Fischer, L., Herrmann, H., Kulmala, M., and Hansel, A.: Accretion Product Formation from Ozonolysis and OH Radical Reaction of alpha-Pinene: Mechanistic Insight and the Influence of Isoprene and Ethylene, Environ. Sci. Technol., 52, 11069-11077, doi: 10.1021/acs.est.8b02210, 2018a.
- 30



- Berndt, T., Scholz, W., Mentler, B., Fischer, L., Herrmann, H., Kulmala, M., and Hansel, A.: Accretion Product Formation from Self- and Cross-Reactions of RO₂ Radicals in the Atmosphere, *Angew. Chem.-International Edition*, 57, 3820-3824, doi: 10.1002/anie.201710989, 2018b.
- Bianchi, F., Tröstl, J., Junninen, H., Frege, C., Henne, S., Hoyle, C. R., Molteni, U., Herrmann, E., Adamov, A., Bukowiecki, N., Chen, X., Duplissy, J., Gysel, M., Hutterli, M., Kangasluoma, J., Kontkanen, J., Kurten, A., Manninen, H. E., Munch, S., Perakyla, O., Petaja, T., Rondo, L., Williamson, C., Weingartner, E., Curtius, J., Worsnop, D. R., Kulmala, M., Dommen, J., and Baltensperger, U.: New particle formation in the free troposphere: A question of chemistry and timing, *Science*, 352, 1109-1112, doi: 10.1126/science.aad5456, 2016.
- Bianchi, F., Kurten, T., Riva, M., Mohr, C., Rissanen, M. P., Roldin, P., Berndt, T., Crouse, J. D., Wennberg, P. O., Mentel, T. F., Wildt, J., Junninen, H., Jokinen, T., Kulmala, M., Worsnop, D. R., Thornton, J. A., Donahue, N., Kjaergaard, H. G., and Ehn, M.: Highly Oxygenated Organic Molecules (HOM) from Gas-Phase Autoxidation Involving Peroxy Radicals: A Key Contributor to Atmospheric Aerosol, *Chemical Reviews*, 119, 3472-3509, doi: 10.1021/acs.chemrev.8b00395, 2019.
- Boyd, C. M., Sanchez, J., Xu, L., Eugene, A. J., Nah, T., Tuet, W. Y., Guzman, M. I., and Ng, N. L.: Secondary organic aerosol formation from the β -pinene+NO₃ system: effect of humidity and peroxy radical fate, *Atmos. Chem. Phys.*, 15, 7497-7522, doi: 10.5194/acp-15-7497-2015, 2015.
- Breitenlechner, M., Fischer, L., Hainer, M., Heinritzi, M., Curtius, J. and Hansel, A.: PTR3: An Instrument for Studying the Lifecycle of Reactive Organic Carbon in the Atmosphere, *Anal. Chem.*, 89, 5825-5832, doi: 10.1021/acs.analchem.6b05110, 2017.
- Browne, E. C., Min, K. E., Wooldridge, P. J., Apel, E., Blake, D. R., Brune, W. H., Cantrell, C. A., Cubison, M. J., Diskin, G. S., Jimenez, J. L., Weinheimer, A. J., Wennberg, P. O., Wisthaler, A. and Cohen, R. C.: Observations of total RONO₂ over the boreal forest: NO_x sinks and HNO₃ sources, *Atmos. Chem. Phys.*, 13, 4543-4562, doi: 10.5194/acp-13-4543-2013, 2013.
- Carlton, A. G., Pinder, R. W., Bhave, P. V., and Pouliot, G. A.: To What Extent Can Biogenic SOA be Controlled?, *Environ. Sci. Technol.*, 44, 3376-3380, doi: 10.1021/es903506b, 2010.
- Capouet, M. and Müller, J. F.: A group contribution method for estimating the vapour pressures of alpha-pinene oxidation products, *Atmos. Chem. Phys.*, 6, 1455-1467, doi: 10.5194/acp-6-1455-2006, 2006.
- Crouse, J. D., Paulot, F., Kjaergaard, H. G., and Wennberg, P. O.: Peroxy radical isomerization in the oxidation of isoprene, *Phys. Chem. Chem. Phys.*, 13, 13607-13613, doi: 10.1039/c1cp21330j, 2011.
- Day, D. A., Liu, S., Russell, L. M., and Ziemann, P. J.: Organonitrate group concentrations in submicron particles with high nitrate and organic fractions in coastal southern California, *Atmos. Environ.*, 44, 1970-1979, doi:10.1016/j.atmosenv.2010.02.045, 2010.



- Eddingsaas, N. C., Loza, C. L., Yee, L. D., Chan, M., Schilling, K. A., Chhabra, P. S., Seinfeld, J. H. and Wennberg, P. O.: alpha-pinene photo-oxidation under controlled chemical conditions - Part 2: SOA yield and composition in low- and high-NO_x environments, *Atmos. Chem. Phys.*, 12, 7413-7427, doi: 10.5194/acp-12-7413-2012, 2012.
- 5 Ehn, M., Kleist, E., Junninen, H., Petaja, T., Lonn, G., Schobesberger, S., Dal Maso, M., Trimborn, A., Kulmala, M., Worsnop, D. R., Wahner, A., Wildt, J. and Mentel, T. F.: Gas phase formation of extremely oxidized pinene reaction products in chamber and ambient air, *Atmos. Chem. Phys.*, 12(11), 5113–5127, doi:10.5194/acp-12-5113-2012, 2012.
- 10 Ehn, M., Thornton, J. A., Kleist, E., Sipilä, M., Junninen, H., Pullinen, I., Springer, M., Rubach, F., Tillmann, R., Lee, B., Lopez-Hilfiker, F., Andres, S., Acir, I.-H., Rissanen, M., Jokinen, T., Schobesberger, S., Kangasluoma, J., Kontkanen, J., Nieminen, T., Kurtén, T., Nielsen, L. B., Jørgensen, S., Kjaergaard, H. G., Canagaratna, M., Dal Maso, M., Berndt, T., Petäjä, T., Wahner, A., Kerminen, V.-M., Kulmala, M., Worsnop, D. R., Wildt, J., and Mentel, T. F.: A large source of low-volatility secondary organic aerosol, *Nature*, 506, 476–479, doi:10.1038/nature13032, 2014.
- 15 Ehn, M., Berndt, T., Wildt, J., and Mentel, T.: Highly Oxygenated Molecules from Atmospheric Autoxidation of Hydrocarbons: A Prominent Challenge for Chemical Kinetics Studies, *International Journal of Chemical Kinetics*, 49, 821-831, doi: 10.1002/kin.21130, 2017.
- Emanuelsson, E. U., Hallquist, M., Kristensen, K., Glasius, M., Bohn, B., Fuchs, H., Kammer, B., Kiendler-Scharr, A., Nehr, S., Rubach, F., Tillmann, R., Wahner, A., Wu, H. C. and Mentel, T. F.: Formation of anthropogenic secondary organic aerosol (SOA) and its influence on biogenic SOA properties, *Atmos. Chem. Phys.*, 13, 2837-2855, doi: 10.5194/acp-13-2837-2013, 2013.
- 20 Farmer, D. K., Matsunaga, A., Docherty, K. S., Surratt, J. D., Seinfeld, J. H., Ziemann, P. J. and Jimenez, J. L.: Response of an aerosol mass spectrometer to organonitrates and organosulfates and implications for atmospheric chemistry, *Proc. Natl. Acad. Sci. U.S.A.*, 107, 6670-6675, doi: 10.1073/pnas.0912340107, 2010.
- Faxon, C., Hammes, J., Le Breton, M., Pathak, R. K., and Hallquist, M.: Characterization of organic nitrate constituents of secondary organic aerosol (SOA) from nitrate-radical-initiated oxidation of limonene using high-resolution chemical ionization mass spectrometry, *Atmos. Chem. Phys.*, 18, 5467-5481, 10.5194/acp-18-5467-2018, 2018..
- 25 Fry, J. L., Draper, D. C., Zarzana, K. J., Campuzano-Jost, P., Day, D. A., Jimenez, J. L., Brown, S. S., Cohen, R. C., Kaser, L., Hansel, A., Cappellin, L., Karl, T., Roux, A. H., Turnipseed, A., Cantrell, C., Lefer, B. L. and Grossberg, N.: Observations of gas- and aerosol-phase organic nitrates at BEACHON-RoMBAS 2011, *Atmos. Chem. Phys.*, 13, 8585-8605, doi: 10.5194/acp-13-8585-2013, 2013.
- 30 Fry, J. L., Draper, D. C., Barsanti, K. C., Smith, J. N., Ortega, J., Winkle, P. M., Lawler, M. J., Brown, S. S., Edwards, P. M., Cohen, R. C. and Lee, L.: Secondary Organic Aerosol formation and organic nitrate yield from NO₃ oxidation of biogenic hydrocarbons, *Environ. Sci. Technol.*, 48, 11944-11953, doi: 10.1021/es502204x, 2014.



- Fuchs, N. A., Sutugin, A. G., Hidy, G. M., and Brock, J. R.: High-dispersed aerosols, *Topics in Current Aerosol Research*, 2, 1-60, doi.org/10.1016/B978-0-08-016674-2.50006-6, 1971.
- Fuller, E. N., Ensley, K., and Giddings, J. C.: Diffusion of halogenated hydrocarbons in helium. Effect of structure on collision cross sections, *J. Phys. Chem.*, 73, 3679- 3685, doi: 10.1021/j100845a020, 1969.
- 5 Glasius, M., la Cour, A. and Lohse, C.: Fossil and nonfossil carbon in fine particulate matter: A study of five European cities, *J. Geophys. Res. Atmos.*, 116, D11302, doi: 10.1029/2011JD015646, 2011.
- de Gouw, J. A., Middlebrook, A. M., Warneke, C., Goldan, P. D., Kuster, W. C., Roberts, J. M., Fehsenfeld, F. C., Worsnop, D. R., Canagaratna, M. R., Pszenny, A. A. P., Keene, W. C., Marchewka, M., Bertman, S. B., and Bates, T. S.: Budget of organic carbon in a polluted atmosphere: Results from the New England Air Quality Study in 2002, *J. Geophys. Res. Atmos.*, 110, D16305, doi: 10.1029/2004jd005623, 2005
- 10 Guenther, A. B., Jiang, X., Heald, C. L., Sakulyanontvittaya, T., Duhl, T., Emmons, L. K., and Wang, X.: The Model of Emissions of Gases and Aerosols from Nature version 2.1 (MEGAN2.1): an extended and updated framework for modeling biogenic emissions, *Geosci. Model Dev.*, 5, 1471–1492, doi:10.5194/gmd-51471-2012, 2012.
- Hallquist, M., Wenger, J. C., Baltensperger, U., Rudich, Y., Simpson, D., Claeys, M., Dommen, J., Donahue, N. M., George, C., Goldstein, A. H., Hamilton, J. F., Herrmann, H., Hoffmann, T., Iinuma, Y., Jang, M., Jenkin, M. E., Jimenez, J. L., Kiendler-Scharr, A., Maenhaut, W., McFiggans, G., Mentel, T. F., Monod, A., Prevot, A. S. H., Seinfeld, J. H., Surratt, J. D., Szmigielski, R. and Wildt, J.: The formation, properties and impact of secondary organic aerosol: current and emerging issues, *Atmos. Chem. Phys.*, 9, 5155-5236, doi: 10.5194/acp-9-5155-2009, 2009.
- 15 Han, Y. M., Stroud, C. A., Liggio, J. and Li, S. M.: The effect of particle acidity on secondary organic aerosol formation from alpha-pinene photooxidation under atmospherically relevant conditions, *Atmos. Chem. Phys.*, 16, 13929-13944, doi: 10.5194/acp-16-13929-2016, 2016.
- Hoyle, C. R., Boy, M., Donahue, N. M., Fry, J. L., Glasius, M., Guenther, A., Hallar, A. G., Hartz, K. H., Petters, M. D., Petaja, T., Rosenoern, T. and Sullivan, A. P.: A review of the anthropogenic influence on biogenic secondary organic aerosol, *Atmos. Chem. Phys.*, 11, 321-343, doi: 10.5194/acp-11-321-2011, 2011.
- 25 Hyttinen, N., Rissanen, M. P., and Kurten, T.: Computational Comparison of Acetate and Nitrate Chemical Ionization of Highly Oxidized Cyclohexene Ozonolysis Intermediates and Products, *Journal of Physical Chemistry A*, 121, 2172-2179, doi: 10.1021/acs.jpca.6b12654, 2017
- Jacobs, M. I., Burke, W. J., and Elrod, M. J.: Kinetics of the reactions of isoprene-derived hydroxynitrates: gas phase epoxide formation and solution phase hydrolysis, *Atmos. Chem. Phys.*, 14, 8933–8946, doi:10.5194/acp-14-8933-2014, 2014.
- 30 Jokinen, T., Berndt, T., Makkonen, R., Kerminen, V. M., Junninen, H., Paasonen, P., Stratmann, F., Herrmann, H., Guenther, A. B., Worsnop, D. R., Kulmala, M., Ehn, M. and Sipila, M.: Production of extremely low volatile organic compounds from biogenic emissions: Measured yields and atmospheric implications, *Proc. Natl. Acad. Sci. U.S.A.*, 112, 7123-7128, doi: 10.1073/pnas.1423977112, 2015.



- Kiendler-Scharr, A., Mensah, A. A., Friese, E., Topping, D., Nemitz, E., Prevot, A. S. H., Äijälä, M., Allan, J., Canonaco, F., Canagaratna, M., Carbone S., Crippa, M., Dall'Osto, M., Day, D. A., De Carlo, P., Di Marco, C. F., Elbern, H., Eriksson, A., Freney, E., Hao, L., Herrmann, H., Hildebrandt, L., Hillamo, R., Jimenez, J. L., Laaksonen, A., McFiggans, G., Mohr, C., O'Dowd, C., Otjes, R., Ovadnevaite, J., Pandis, S. N., Poulain, L., Schlag, P., Sellegri, K., Swietlicki, E., Tiitta, P., Vermeulen, A., Wahner, A., Worsnop, D., and Wu, H.-C.: Ubiquity of organic nitrates from nighttime chemistry in the European submicron aerosol, *Geophys. Res. Lett.*, 43, 7735 – 7744, doi:10.1002/2016GL069239, 2016.
- Kim, H., Barkey, B. and Paulson, S. E.: Real Refractive Indices and Formation Yields of Secondary Organic Aerosol Generated from Photooxidation of Limonene and alpha-Pinene: The Effect of the HC/NO_x Ratio, *J. Phys. Chem. A*, 116, 6059-6067, doi: 10.1021/jp301302z, 2012.
- Kirkby, J., Duplissy, J., Sengupta, K., Frege, C., Gordon, H., Williamson, C., Heinritzi, M., Simon, M., Yan, C., Almeida, J., Tröstl, J., Nieminen, T., Ortega, I. K., Wagner, R., Adamov, A., Amorim, A., Bernhammer, A. K., Bianchi, F., Breitenlechner, M., Brilke, S., Chen, X. M., Craven, J., Dias, A., Ehrhart, S., Flagan, R. C., Franchin, A., Fuchs, C., Guida, R., Hakala, J., Hoyle, C. R., Jokinen, T., Junninen, H., Kangasluoma, J., Kim, J., Krapf, M., Kurten, A., Laaksonen, A., Lehtipalo, K., Makhmutov, V., Mathot, S., Molteni, U., Onnela, A., Perakyla, O., Piel, F., Petaja, T., Praplan, A. P., Pringle, K., Rap, A., Richards, N. A. D., Riipinen, I., Rissanen, M. P., Rondo, L., Sarnela, N., Schobesberger, S., Scott, C. E., Seinfeld, J. H., Sipila, M., Steiner, G., Stozhkov, Y., Stratmann, F., Tome, A., Virtanen, A., Vogel, A. L., Wagner, A. C., Wagner, P. E., Weingartner, E., Wimmer, D., Winkler, P. M., Ye, P. L., Zhang, X., Hansel, A., Dommen, J., Donahue, N. M., Worsnop, D. R., Baltensperger, U., Kulmala, M., Carslaw, K. S., Curtius, J.: Ion-induced nucleation of pure biogenic particles, *Nature*, 533, 521–526, doi: 10.1038/nature17953, 2016.
- Kroll, J. H., Ng, N. L., Murphy, S. M., Flagan, R. C. and Seinfeld, J. H.: Secondary organic aerosol formation from isoprene photo-oxidation, *Environ. Sci. Technol.*, 40, 1869-1877, doi: 10.1021/es0524301, 2006.
- Lee, A. K. Y., Abbatt, J. P. D., Leaitch, W. R., Li, S. M., Sjostedt, S. J., Wentzell, J. J. B., Liggio, J., and Macdonald, A. M.: Substantial secondary organic aerosol formation in a coniferous forest: observations of both day- and nighttime chemistry, *Atmos. Chem. Phys.*, 16, 6721-6733, doi: 10.5194/acp-16-6721-2016, 2016a.
- Lee, B. H., Mohr, C., Lopez-Hilfiker, F. D., Lutz, A., Hallquist, M., Lee, L., Romer, P., Cohen, R. C., Iyer, S., Kurten, T., Hu, W. W., Day, D. A., Campuzano-Jost, P., Jimenez, J. L., Xu, L., Ng, N. L., Guo, H. Y., Weber, R. J., Wild, R. J., Brown, S. S., Koss, A., de Gouw, J., Olson, K., Goldstein, A. H., Seco, R., Kim, S., McAvey, K., Shepson, P. B., Starn, T., Baumann, K., Edgerton, E. S., Liu, J. M., Shilling, J. E., Miller, D. O., Brune, W., Schobesberger, S., D'Ambro, E. L. and Thornton, J. A.: Highly functionalized organic nitrates in the southeast United States: Contribution to secondary organic aerosol and reactive nitrogen budgets, *Proc. Natl. Acad. Sci. U.S.A.*, 113, 1516-1521, doi: 10.1073/pnas.1508108113, 2016b.



- Lehtipalo, K., Yan, C., Dada, L., Bianchi, F., Xiao, M., Wagner, R., Stolzenburg, D., Ahonen, L. R., Amorim, A., Baccarini, A., Bauer, P. S., Baumgartner, B., Bergen, A., Bernhammer, A. K., Breitenlechner, M., Brilke, S., Buchholz, A., Mazon, S. B., Chen, D. X., Chen, X. M., Dias, A., Dommen, J., Draper, D. C., Duplissy, J., Ehn, M., Finkenzeller, H., Fischer, L., Frege, C., Fuchs, C., Garmash, O., Gordon, H., Hakala, J., He, X. C., Heikkinen, L., Heinritzi, M., Helm, J. C., Hofbauer, V., Hoyle, C. R., Jokinen, T., Kangasluoma, J., Kerminen, V. M., Kim, C., Kirkby, J., Kontkanen, J., Kurten, A., Lawler, M. J., Mai, H. J., Mathot, S., Mauldin, R. L., Molteni, U., Nichman, L., Nie, W., Nieminen, T., Ojdanic, A., Onnela, A., Passananti, M., Petaja, T., Piel, F., Pospisilova, V., Quelever, L. L. J., Rissanen, M. P., Rose, C., Sarnela, N., Schallhart, S., Schuchmann, S., Sengupta, K., Simon, M., Sipila, M., Tauber, C., Tome, A., Trostl, J., Vaisanen, O., Vogel, A. L., Volkamer, R., Wagner, A. C., Wang, M. Y., Weitz, L., Wimmer, D., Ye, P. L., Ylisirnio, A., Zha, Q. Z., Carslaw, K. S., Curtius, J., Donahue, N. M., Flagan, R. C., Hansel, A., Riipinen, I., Virtanen, A., Winkler, P. M., Baltensperger, U., Kulmala, M., and Worsnop, D. R.: Multicomponent new particle formation from sulfuric acid, ammonia, and biogenic vapors, *Science Advances*, 4, doi: 10.1126/sciadv.aau5363, 2018.
- Liu, S., Shilling, J. E., Song, C., Hiranuma, N., Zaveri, R. A., and Russell, L. M.: Hydrolysis of organonitrate functional groups in aerosol particles, *Aerosol Sci. Tech.*, 46, 1359–1369, doi:10.1080/02786826.2012.716175, 2012.
- McFiggans, G., Mentel, T. F., Wildt, J., Pullinen, I., Kang, S., Kleist, E., Schmitt, S., Springer, M., Tillmann, R., Wu, C., Zhao, D., Hallquist, M., Faxon, C., Le Breton, M., Hallquist, Å. M., Simpson, D., Bergström, R., Jenkin, M. E., Ehn, M., Thornton, J. A., Alfarra, M. R., Bannan, T. J., Percival, C. J., Priestley, M., Topping, D., and Kiendler-Scharr, A.: Secondary organic aerosol reduced by mixture of atmospheric vapours, *Nature*, 565, 587–593, doi: 10.1038/s41586-018-0871-y, 2019.
- Mentel, T. F., Wildt, J., Kiendler-Scharr, A., Kleist, E., Tillmann, R., Dal Maso, M., Fisseha, R., Hohaus, T., Spahn, H., Uerlings, R., Wegener, R., Griffiths, P. T., Dinar, E., Rudich, Y. and Wahner, A.: Photochemical production of aerosols from real plant emissions, *Atmos. Chem. Phys.*, 9, 4387–4406, doi: 10.5194/acpd-9-3041-2009, 2009.
- Mentel, T. F., Kleist, E., Andres, S., Dal Maso, M., Hohaus, T., Kiendler-Scharr, A., Rudich, Y., Springer, M., Tillmann, R., Uerlings, R., Wahner, A. and Wildt, J.: Secondary aerosol formation from stress-induced biogenic emissions and possible climate feedbacks, *Atmos. Chem. Phys.*, 13, 8755–8770, doi: 10.5194/acp-13-8755-2013, 2013.
- Mentel, T. F., Springer, M., Ehn, M., Kleist, E., Pullinen, I., Kurtén, T., Rissanen, M., Wahner, A., and Wildt, J.: Formation of highly oxidized multifunctional compounds: autoxidation of peroxy radicals formed in the ozonolysis of alkenes – deduced from structure-product relationships, *Atmos. Chem. Phys.*, 15, 6745– 6765, doi:10.5194/acp-15-6745-2015, 2015.
- Mutzel, A., Poulain, L., Berndt, T., Iinuma, Y., Rodigast, M., Boge, O., Richters, S., Spindler, G., Sipila, M., Jokinen, T., Kulmala, M. and Herrmann, H.: Highly Oxidized Multifunctional Organic Compounds Observed in Tropospheric Particles: A Field and Laboratory Study, *Environ. Sci. Technol.*, 49, 7754–7761, doi: 10.1021/acs.est.5b00885, 2015.



- Ng, N. L., Chhabra, P. S., Chan, A. W. H., Surratt, J. D., Kroll, J. H., Kwan, A. J., McCabe, D. C., Wennberg, P. O., Sorooshian, A., Murphy, S. M., Dalleska, N. F., Flagan, R. C. and Seinfeld, J. H.: Effect of NO_x level on secondary organic aerosol (SOA) formation from the photo-oxidation of terpenes, *Atmos. Chem. Phys.*, 7, 5159-5174, doi: 10.5194/acpd-7-10131-2007, 2007.
- 5 Noziere, B., Barnes, I. and Becker, K. H.: Product study and mechanisms of the reactions of alpha-pinene and of pinonaldehyde with OH radicals. *J. Geophys. Res. Atmos.*, 104, 23645– 23656, doi: 10.1029/1999JD900778, 1999.
- Pandis, S. N., Paulson, S. E., Seinfeld, J. H. and Flagan, R. C.: Aerosol formation in the photo-oxidation of isoprene and beta-pinene, *Atmos. Environ. Part A*, 25, 997-1008, doi: 10.1016/0960-1686(91)90141-S, 1991.
- Pankow, J. F. and Asher, W. E.: SIMPOL.1: a simple group contribution method for predicting vapor pressures and enthalpies of vaporization of multifunctional organic compounds, *Atmos. Chem. Phys.*, 8, 2773–2796, doi:10.5194/acp-8-27732008, 2008.
- 10 Peräkylä, O., Riva, M., Heikkinen, L., Quéléver, L., Roldin, P., and Ehn, M.: Experimental investigation into the volatilities of highly oxygenated organic molecules (HOM), *Atmos. Chem. Phys. Discuss.*, 2019, 1-28, doi: 10.5194/acp-2019-620, 2019.
- 15 Presto, A. A., Hartz, K. E. H., and Donahue, N. M.: Secondary organic aerosol production from terpene ozonolysis. 2. Effect of NO_x concentration, *Environ. Sci. Technol.*, 39, 7046-7054, 10.1021/es050400s, 2005.
- Pullinen, I.: Photochemistry of Highly Oxidized Multifunctional Organic Molecules: a Chamber Study, *Mathematisch-Naturwissenschaftliche Fakultät, Köln, Schriften des Forschungszentrums Jülich Reihe Energie & Umwelt / Energy & Environment*, 2017.
- 20 Rindelaub, J. D., McAvey, K. M., and Shepson, P. B.: The photochemical production of organic nitrates from alpha-pinene and loss via acid-dependent particle phase hydrolysis, *Atmos. Environ.*, 100, 193–201, doi:10.1016/j.atmosenv.2014.11.010, 2015.
- Rindelaub, J. D., Borca, C. H., Hostetler, M. A., Slade, J. H., Lipton, M. A., Slipchenko, L. V. and Shepson, P. B.: The acid-catalyzed hydrolysis of an alpha-pinene-derived organic nitrate: kinetics, products, reaction mechanisms, and atmospheric impact, *Atmos. Chem. Phys.*, 16, 15425-15432, doi: 10.5194/acp-16-15425-2016, 2016.
- 25 Rissanen, M. P.: NO₂ Suppression of Autoxidation–Inhibition of Gas-Phase Highly Oxidized Dimer Product Formation, *ACS Earth and Space Chemistry*, 2, 1211-1219, doi: 10.1021/acsearthspacechem.8b00123, 2018.
- Rissanen, M. P., Kurten, T., Sipilä, M., Thornton, J. A., Kangasluoma, J., Sarnela, N., Junninen, H., Jorgensen, S., Schallhart, S., Kajos, M. K., Taipale, R., Springer, M., Mentel, T. F., Ruuskanen, T., Petaja, T., Worsnop, D. R., Kjaergaard, H. G., and Ehn, M.: The Formation of Highly Oxidized Multifunctional Products in the Ozonolysis of Cyclohexene, *Journal of the American Chemical Society*, 136, 15596-15606, doi: 10.1021/ja507146s, 2014.
- 30 Riva, M., Rantala, P., Krechmer, J. E., Perakyla, O., Zhang, Y. J., Heikkinen, L., Garmash, O., Yan, C., Kulmala, M., Worsnop, D., and Ehn, M.: Evaluating the performance of five different chemical ionization techniques for



- detecting gaseous oxygenated organic species, *Atmospheric Measurement Techniques*, 12, 2403-2421, 10.5194/amt-12-2403-2019, 2019.
- Rollins, A. W., Smith, J. D., Wilson, K. R. and Cohen, R. C.: Real time in situ detection of organic nitrates in atmospheric aerosols. *Environ. Sci. Technol.*, 44, doi: 10.1021/es100926x, 5540–5545, 2010.
- 5 Romer, P. S., Duffey, K. C., Wooldridge, P. J., Allen, H. M., Ayres, B. R., Brown, S. S., Brune, W. H., Crounse, J. D., de Gouw, J., Draper, D. C., Feiner, P. A., Fry, J. L., Goldstein, A. H., Koss, A., Misztal, P. K., Nguyen, T. B., Olson, K., Teng, A. P., Wennberg, P. O., Wild, R. J., Zhang, L. and Cohen, R. C.: The lifetime of nitrogen oxides in an isoprene-dominated forest, *Atmos. Chem. Phys.*, 16, 7623-7637, doi: 10.5194/acp-16-7623-2016, 2016.
- Rubach, F.: Aerosol processes in the Planetary Boundary Layer: High resolution Aerosol Mass Spectrometry on a Zeppelin
10 NT Airship, Fachgruppe Chemie und Biologie, Physikalische und Theoretische Chemie, Universität Wuppertal, Schriften des Forschungszentrums Jülich, Reihe Energie & Umwelt / Energy & Environment, Band / Volume 196, 2013.
- Sarrafzadeh, M., Wildt, J., Pullinen, I., Springer, M., Kleist, E., Tillmann, R., Schmitt, S. H., Wu, C., Mentel, T. F., Zhao, D., Hastie, D. R. and Kiendler-Scharr, A.: Impact of NO_x and OH on secondary organic aerosol formation from β-pinene photo-oxidation, *Atmos. Chem. Phys.*, 16, 11237-11248, doi: 10.5194/acp-16-11237-2016, 2016.
- 15 Shilling, J. E., Zaveri, R. A., Fast, J. D., Kleinman, L., Alexander, M. L., Canagaratna, M. R., Fortner, E., Hubbe, J. M., Jayne, J. T., Sedlacek, A., Setyan, A., Springston, S., Worsnop, D. R. and Zhang, Q.: Enhanced SOA formation from mixed anthropogenic and biogenic emissions during the CARES campaign, *Atmos. Chem. Phys.*, 13, 2091-2113, doi: 10.5194/acp-13-2091-2013, 2013.
- 20 Spracklen, D. V., Jimenez, J. L., Carslaw, K. S., Worsnop, D. R., Evans, M. J., Mann, G. W., Zhang, Q., Canagaratna, M. R., Allan, J., Coe, H., McFiggans, G., Rap, A., and Forster, P.: Aerosol mass spectrometer constraint on the global secondary organic aerosol budget, *Atmos. Chem. Phys.*, 11, 12109-12136, doi: 10.5194/acp-11-12109-2011, 2011
- Stirnweis, L., Marcolli, C., Dommen, J., Barmet, P., Frege, C., Platt, S. M., Bruns, E. A., Krapf, M., Slowik, J. G., Wolf, R., Prévôt, A. S. H., Baltensperger, U. and El-Haddad, I.: Assessing the influence of NO_x concentrations and relative
25 humidity on secondary organic aerosol yields from α-pinene photo-oxidation through smog chamber experiments and modelling calculations, *Atmos. Chem. Phys.*, 17, 5035-5061, doi: 10.5194/acp-17-5035-2017, 2017.
- Tröstl, J., Chuang, W. K., Gordon, H., Heinritzi, M., Yan, C., Molteni, U., Ahlm, L., Frege, C., Bianchi, F., Wagner, R., Simon, M., Lehtipalo, K., Williamson, C., Craven, J. S., Duplissy, J., Adamov, A., Almeida, J., Bernhammer, A. K., Breitenlechner, M., Brilke, S., Dias, A., Ehrhart, S., Flagan, R. C., Franchin, A., Fuchs, C., Guida, R., Gysel, M., Hansel, A., Hoyle, C. R., Jokinen, T., Junninen, H., Kangasluoma, J., Keskinen, H., Kim, J., Krapf, M., Kurten, A., Laaksonen, A., Lawler, M., Leiminger, M., Mathot, S., Mohler, O., Nieminen, T., Onnela, A., Petaja, T., Piel, F. M., Miettinen, P., Rissanen, M. P., Rondo, L., Sarnela, N., Schobesberger, S., Sengupta, K., Sipila, M., Smith, J. N., Steiner, G., Tome, A., Virtanen, A., Wagner, A. C., Weingartner, E., Wimmer, D., Winkler, P. M., Ye, P. L., Carslaw, K. S., Curtius, J., Dommen, J., Kirkby, J., Kulmala, M., Riipinen, I., Worsnop, D. R., Donahue, N. M., and



- Baltensperger, U.: The role of low-volatility organic compounds in initial particle growth in the atmosphere, *Nature*, 533, 527-531, doi: 10.1038/nature18271, 2016.
- Wildt, J., Mentel, T. F., Kiendler-Scharr, A., Hoffmann, T., Andres, S., Ehn, M., Kleist, E., Muesgen, P., Rohrer, F., Rudich, Y., Springer, M., Tillmann, R. and Wahner, A.: Suppression of new particle formation from monoterpene oxidation by NO_x, *Atmos. Chem. Phys.*, 14, 2789–2804, doi:10.5194/acp-14-2789-2014, 2014.
- Worton, D. R., Goldstein, A. H., Farmer, D. K., Docherty, K. S., Jimenez, J. L., Gilman, J. B., Kuster, W. C., de Gouw, J., Williams, B. J., Kreisberg, N. M., Hering, S. V., Bench, G., McKay, M., Kristensen, K., Glasius, M., Surratt, J. D. and Seinfeld, J. H.: Origins and composition of fine atmospheric carbonaceous aerosol in the Sierra Nevada Mountains, California, *Atmos. Chem. Phys.*, 11, 10219-10241, doi: 10.5194/acp-11-10219-2011, 2011.
- Valiev, R. R., Hasan, G., Salo, V. T., Kubecka, J., and Kurten, T.: Intersystem Crossings Drive Atmospheric Gas-Phase Dimer Formation, *J. Phys. Chem. A*, 123, 6596-6604, 10.1021/acs.jpca.9b02559, 2019.
- Xu, L., Guo, H. Y., Boyd, C. M., Klein, M., Bougiatioti, A., Cerully, K. M., Hite, J. R., Isaacman-VanWertz, G., Kreisberg, N. M., Knote, C., Olson, K., Koss, A., Goldstein, A. H., Hering, S. V., de Gouw, J., Baumann, K., Lee, S. H., Nenes, A., Weber, R. J. and Ng, N. L.: Effects of anthropogenic emissions on aerosol formation from isoprene and monoterpenes in the southeastern United States, *Proc. Natl. Acad. Sci. U.S.A.*, 112, 37-42, doi: 10.1073/pnas.1417609112, 2015a.
- Xu, L., Suresh, S., Guo, H., Weber, R. J. and Ng, N. L.: Aerosol characterization over the southeastern United States using high resolution aerosol mass spectrometry: spatial and seasonal variation of aerosol composition and sources with a focus on organic nitrates. *Atmos. Chem. Phys.*, 15, 7307–7336, doi: 10.5194/acp-15-7307-2015, 2015b.
- Zhang, J. Y., Hartz, K. E. H., Pandis, S. N. and Donahue, N. M.: Secondary organic aerosol formation from limonene ozonolysis: Homogeneous and heterogeneous influences as a function of NO_x, *J. Phys. Chem. A*, 110, 11053-11063, doi: 10.1021/jp062836f, 2006.
- Zhang, X., Lambe, A. T., Upshur, M. A., Brooks, W. A., Be, A. G., Thomson, R. J., Geiger, F. M., Surratt, J. D., Zhang, Z. F., Gold, A., Graf, S., Cubison, M. J., Groessl, M., Jayne, J. T., Worsnop, D. R. and Canagaratna, M. R.: Highly Oxygenated Multifunctional Compounds in alpha-Pinene Secondary Organic Aerosol, *Environ. Sci. Technol.*, 51, 5932-5940, doi: 10.1021/acs.est.6b06588, 2017.
- Zhao, D., Schmitt, S. H., Wang, M., Acir, I. H., Tillmann, R., Tan, Z., Novelli, A., Fuchs, H., Pullinen, I., Wegener, R., Rohrer, F., Wildt, J., Kiendler-Scharr, A., Wahner, A., and Mentel, T. F.: Effects of NO_x and SO₂ on the secondary organic aerosol formation from photooxidation of α -pinene and limonene, *Atmos. Chem. Phys.*, 18, 1611-1628, doi: 10.5194/acp-18-1611-2018, 2018.



Tables

Table 1: Overview of α -pinene and β -pinene experiments

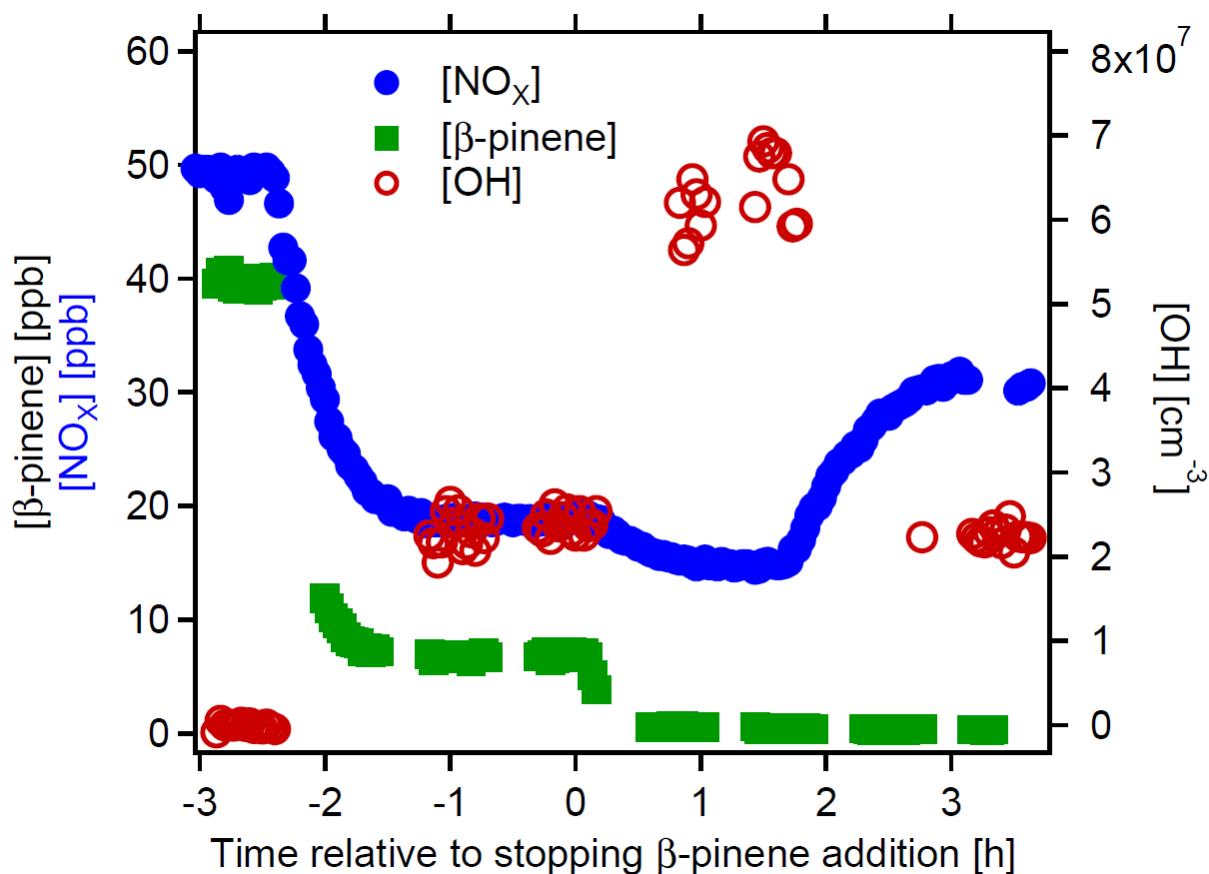
5

Experiment Description	[VOC] ₀ [ppb]	[NO _x] ₀ [ppb]
1. Gas-phase yield of ON and OrgNO ₃ (Section 3.1)	β -pinene 39→0 m-xylene 3.7	50
2. Formation of HOM-ON (Section 3.3)	α -pinene 12 β -pinene 37	0.3 / 15.5 / 26.7 / 39.7 / 59.1 / 83.3 / 137.8 0.3 / 3.9 / 53.8 / 113.6 / 194
3. Effective uptake coefficients* (Section 3.4)	α -pinene 12.5 β -pinene 37	0.3 52.5
4. OrgNO ₃ in SOA (Section 3.5)	α -pinene 46 β -pinene 37	0.3 / 32 / 51 / 60 0.3 / 6.7 / 13.4 / 32.9 / 54.8 / 103

*in presence of ammonium sulfate seed aerosols



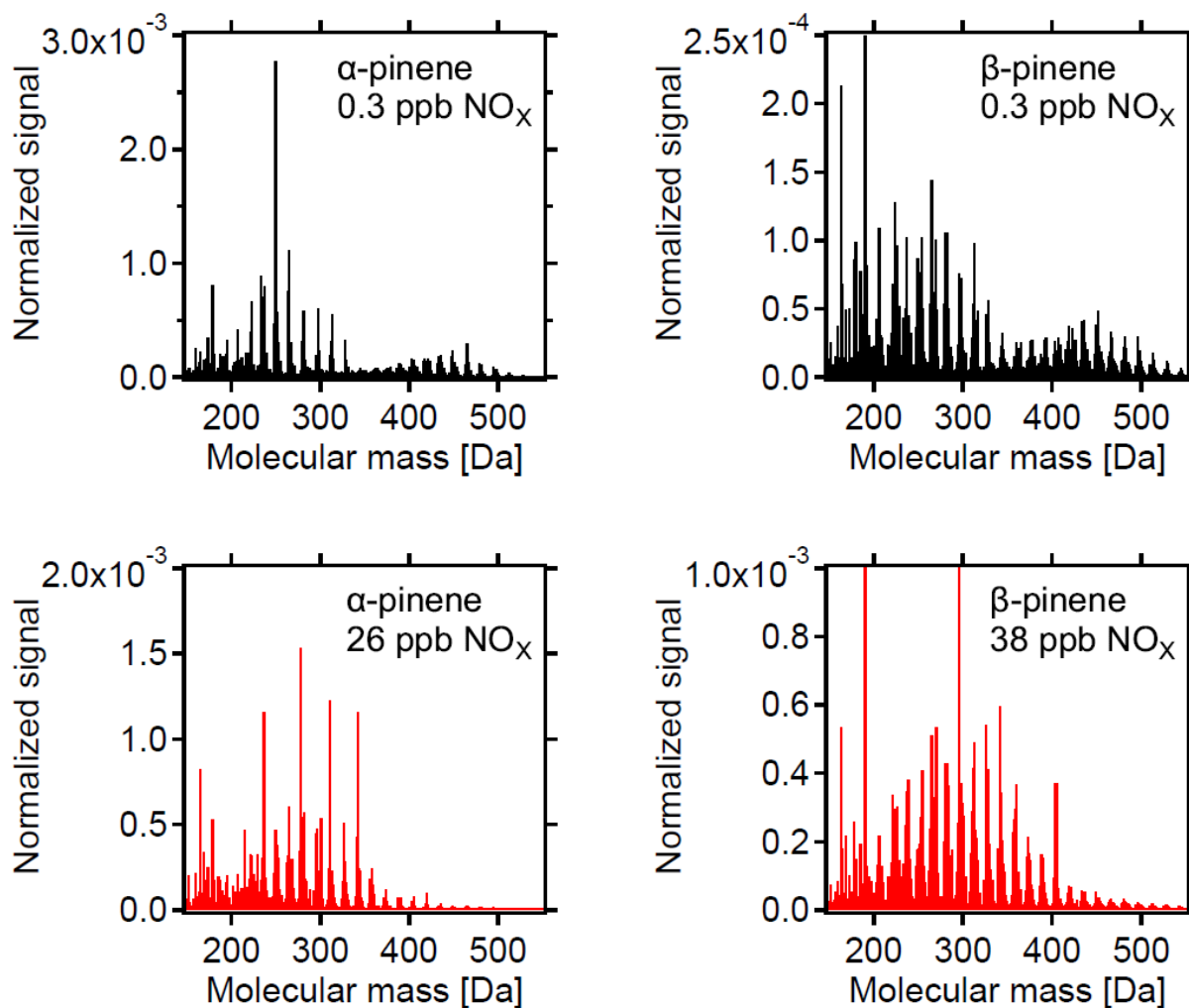
Figures



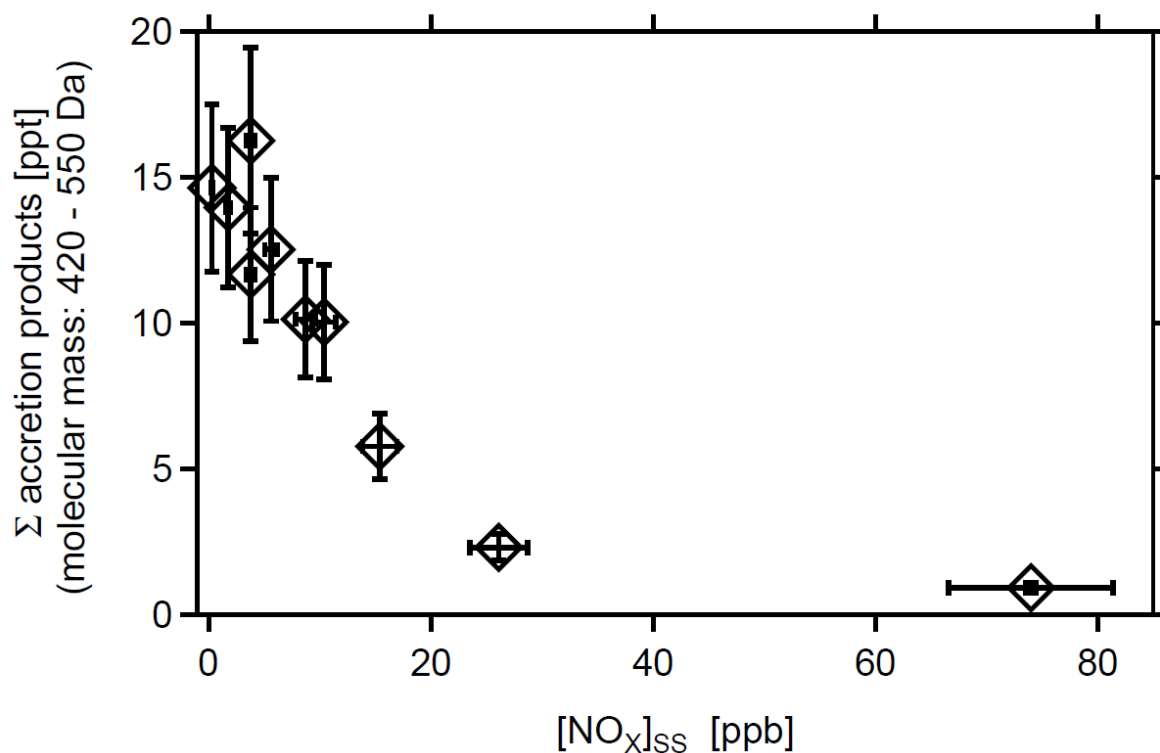
5

Figure 1: Time series of $[\beta\text{-pinene}]$ (green squares, left scale), $[\text{NO}_x]$ (blue circles, left scale) and $[\text{OH}]$ (open brown circles, right scale). The experiment served to estimate the sum of organic nitrates (ON) formed in a mix of NO_x and β -pinene. *m*-xylene ($[\text{m-xylene}]_0 \sim 3.7$ ppb) was added to the chamber as tracer for OH. At time $t = -2.4$ h OH formation was induced by O_3 photolysis. At time $t = 0$ h, β -pinene addition was stopped and at time $t = 1.7$ h $J(\text{O}^1\text{D})$ was reduced to obtain the same $[\text{OH}]$ as in presence of β -pinene at time -1 h.

10

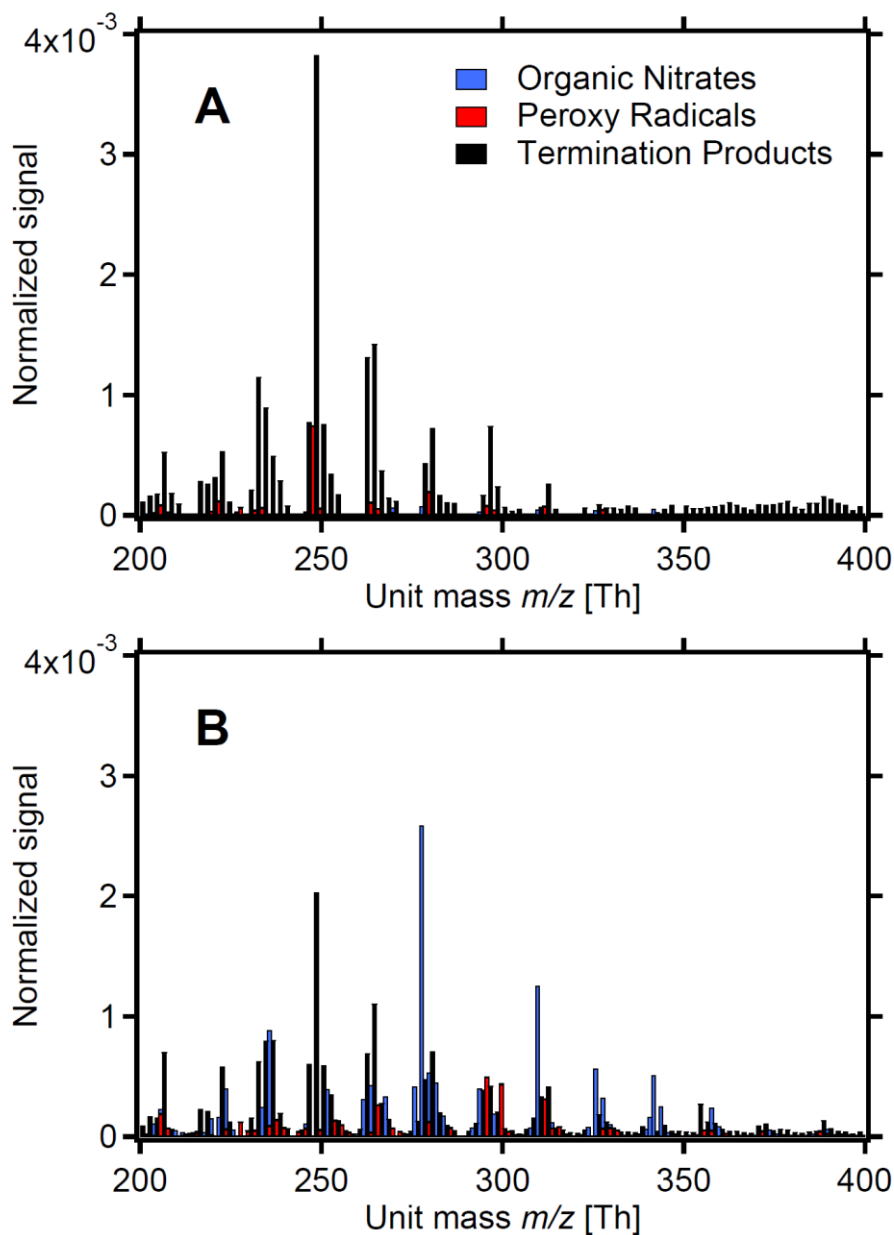


5 **Figure 2.** HOM spectra from photo-oxidation of α -pinene (left panels) and β -pinene (right panels) without NO_x addition (upper panels) and with NO_x addition (lower panels). NO_x concentrations in the α -pinene and β -pinene experiment were 26 ppb and 38 ppb, respectively. Background NO_x was 0.3ppb.

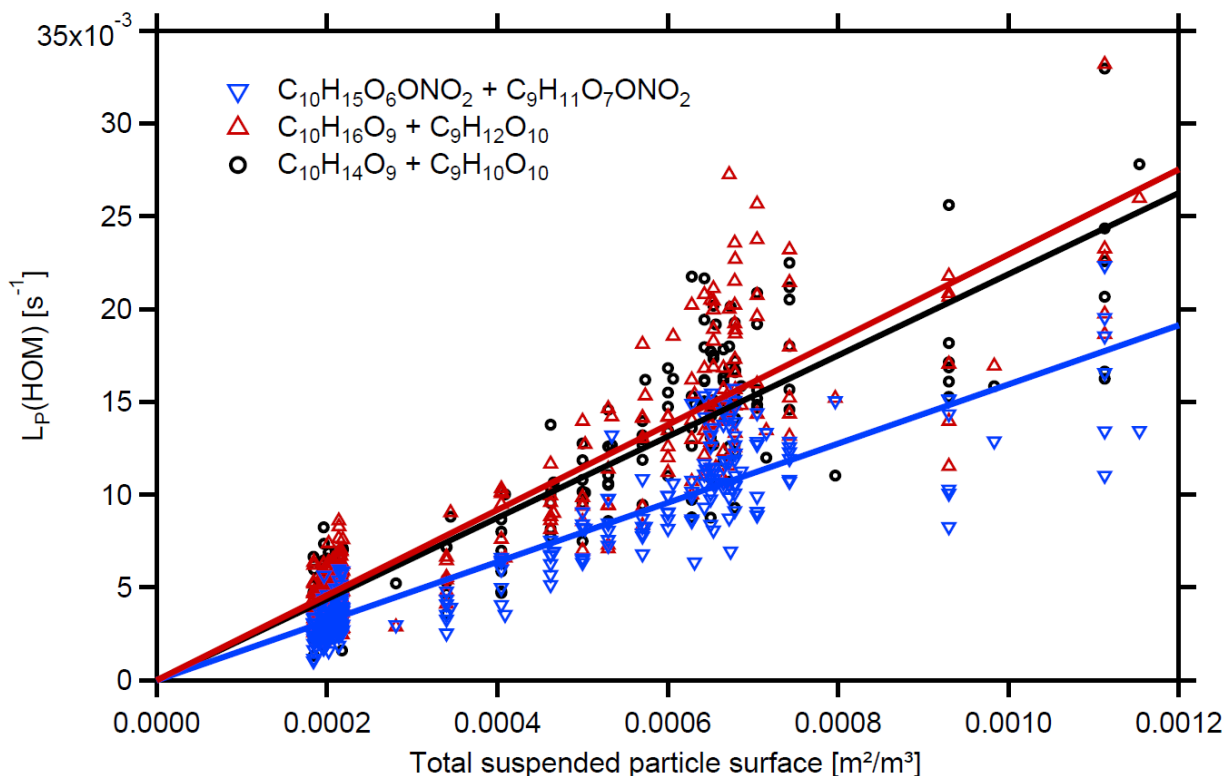


5 **Figure 3.** Mixing ratio of the sum HOM accretion products with molecular masses from 420 to 550 Da in dependence of [NO_x] in an *α*-pinene photo-oxidation experiment. Mixing ratios were corrected as described in supplement section S1.2. Observed particle surface ranged from $\sim 10^{-6}$ m²m⁻³ to 4.0×10^{-5} m²m⁻³ resulting in correction factors between 1.0 and 1.17. Turnover ranged from 8.7×10^7 cm⁻³s⁻¹ and 1.04×10^8 cm⁻³s⁻¹ leading to correction factors in a range of 1.2 - 0.8. The correction factors were close to one thus did not add much uncertainty.

10



5 Figure 4: HOM pattern from α -pinene photo-oxidation at two NO_x levels in the monomer range. Upper panel low NO_x conditions ($[\alpha\text{-pinene}]_{\text{SS}} = 1.7$ ppb, $[\text{NO}_x]_{\text{SS}} = 0.3$ ppb), lower panel high NO_x conditions ($[\alpha\text{-pinene}]_{\text{SS}} = 1.0$ ppb, $[\text{NO}_x]_{\text{SS}} = 8.7$ ppb). Black bars = HOM-PP = termination products of reactions R3 and R4. Blue bars = HOM-ON = organic nitrates. Red bars = HOM-RO2 (peroxy radicals). The signals were normalized to the sum over all detected ions.



5 **Figure 5:** Plot of $L_p(\text{HOM})$ calculated by Eq.(6) versus particle surface, S_p , for the examples of HOM-ON with a molecular mass of = 293 Da ($\text{C}_{10}\text{H}_{15}\text{O}_6\text{ONO}_2$ & $\text{C}_9\text{H}_{11}\text{O}_7\text{ONO}_2$), HOM-PP with a molecular mass of 280 Da ($\text{C}_{10}\text{H}_{16}\text{O}_9$ and $\text{C}_9\text{H}_{12}\text{O}_{10}$), and HOM-PP with molecular mass of 278 ($\text{C}_{10}\text{H}_{14}\text{O}_9$ and $\text{C}_9\text{H}_{10}\text{O}_{10}$). HOM from β -pinene photo-oxidation ($[\beta\text{-pinene}]_{\text{SS}} \sim 10$ ppb, $[\text{NOx}]_{\text{SS}} \sim 4$ ppb). Dividing the slopes by the respective $\sqrt[3]{4}$ led to $f_{\text{FS}} \cdot \gamma_{\text{eff}} \sim 0.5$ for the example HOM-ON and ~ 0.6 in the latter cases. The main uncertainty arises from the scatter of $L_p(\text{HOM})$ individual unit mass resolution data. Statistical errors of $f_{\text{FS}} \cdot \gamma_{\text{eff}}$ were about $\pm 5\%$.

10

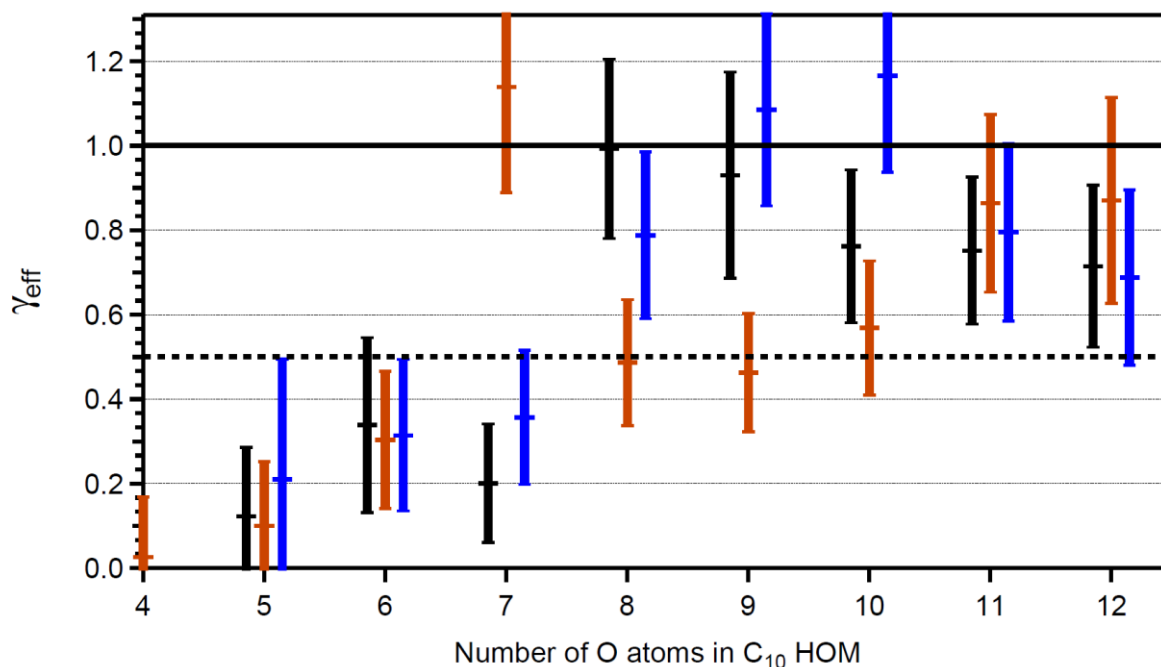
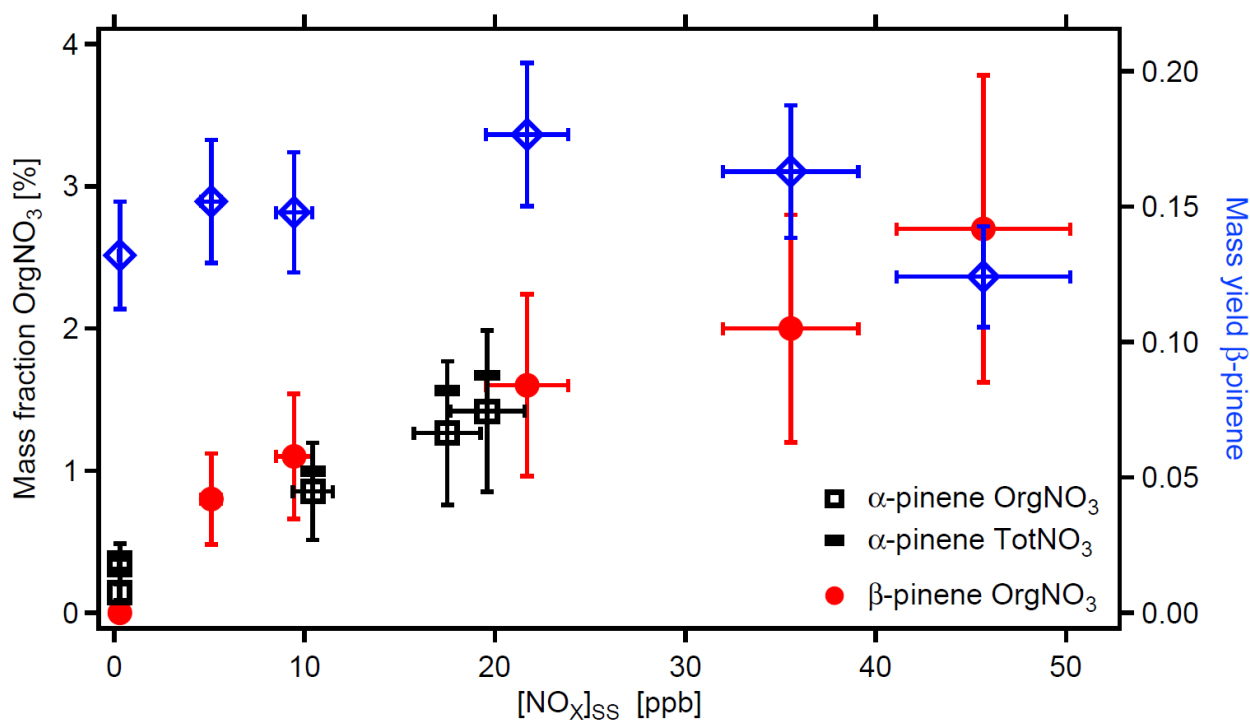
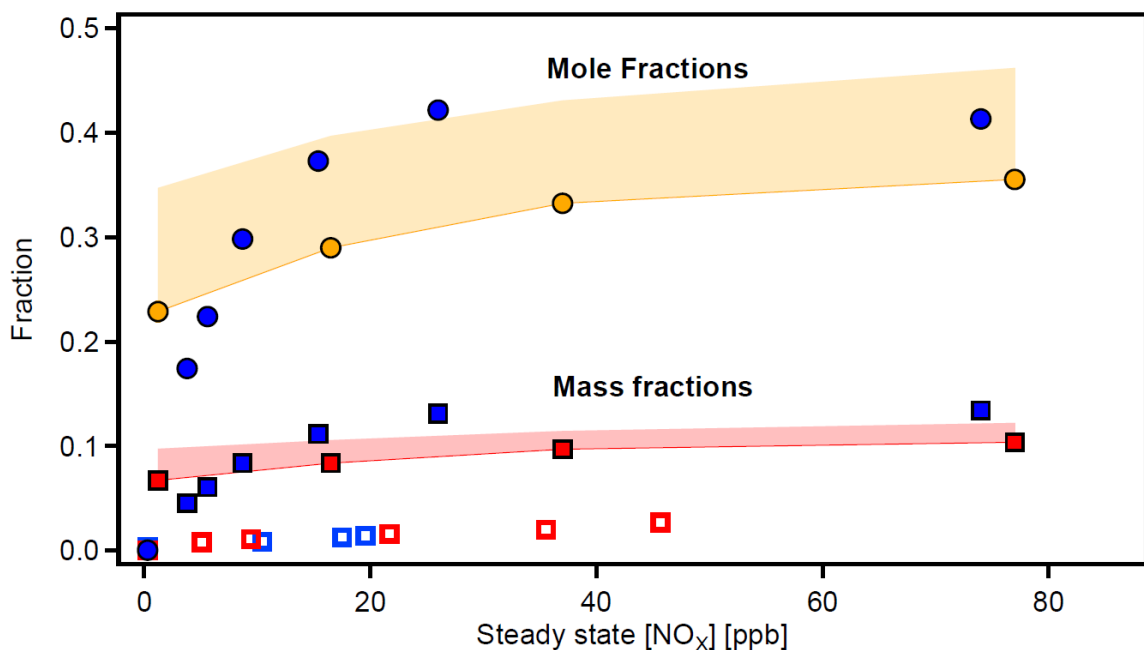


Figure 6: Effective uptake coefficients γ_{eff} for HOM-PP ($C_{10}H_{14}O_x$ black bars, $C_{10}H_{16}O_x$, brown bars) and HOM-ON ($C_{10}H_{15}O_xNO_2$, blue bars) in dependence of the number of O atoms in the respective HOM. HOM with different numbers of C, H, and O atoms, e.g. $C_{10}H_yO_x$ and $C_9H_{y-4}O_{x+1}$ HOM-PP, are treated together and the number of O-atoms is given for the C_{10} -HOM-PP. The second component, C_9 -HOM-PP, has one O atom more. Data were taken from β -pinene photo-oxidation experiment with $[\beta\text{-pinene}]_{SS} \sim 10$ ppb, $[NO_x]_{SS} \sim 4$ ppb. The signal intensity for the $C_{10}H_{14}O_4$ and HOM-ON with 4 O-atoms was too low to allow reliable determination of γ_{eff} and the respective data is left out. Uncertainties in γ_{eff} arise from the determination procedure as shown in Figure 5. The black line indicates $\gamma_{eff} = 1$ and 0.5. An average Fuchs-Sutugin correction factor of 0.70 ($d_p = 175$ nm) was applied to calculate γ_{eff} .

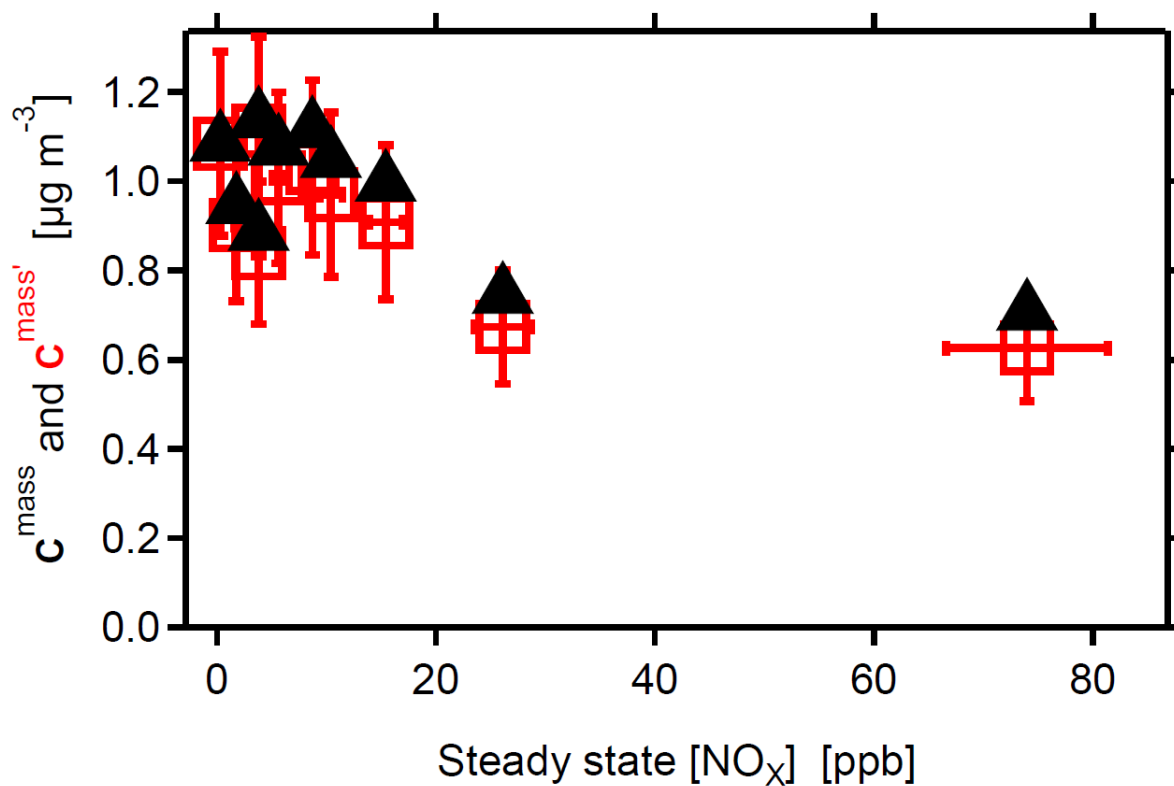


5 Figure 7: Mass fraction of organic bound nitrate (OrgNO₃) in SOA in dependence of [NO_x]_{ss} (left y-axis). Black squares and red
circles show data measured from α-pinene and β-pinene, respectively. Yields of SOA mass formation during the respective
experiment are shown at the example of β-pinene (blue diamonds). The data are corrected for wall losses of HOM. In absence of
OH, [α-pinene]₀ was around 46 ppb, [β-pinene]₀ was around 37 ppb. NO_x was added at different amounts with [NO_x]₀ up to 103
ppb. Due to losses in reactions with OH and formation of organic nitrates, [NO_x] decreased to the [NO_x]_{ss} levels shown here.
10 Uncertainties in NO_x data are estimated to ± 10%, uncertainties in SOA masses to ± 10 %, and uncertainties in the content of
OrgNO₃ are estimated to ± 40%. The black bars indicate the fraction of total nitrate (TotNO₃, left scale) for the example of α-
pinene, which is dominated by organic nitrate.



5 **Figure 8:** Molecular fraction of HOM-ON (filled spheres) and mass ratio (squares) as a function of $[\text{NO}_x]_{\text{SS}}$. Data from α -pinene (blue symbols) and β -pinene (orange and red symbols and areas). We were able to assign molecular formulas to more than 90% of the signal and the analysis in Figure 6 is based on the assigned peaks (supplement, Table S1). The mass fraction of OrgNO_3 in the gas-phase HOM is significantly higher than in the particulate phase as determined by AMS (open blue and red squares). The areas in orange and red give the potential error for β -pinene due to unresolved progressions and overlap of organic nitrates with peroxy radicals (as explained in text).

10



5 **Figure 9.** Mass concentrations for the sum of all HOM with molar weights between 230 to 550 Da. Black triangles show mass concentrations c^{mass} as determined. Red squares show c^{mass} , i.e. the resulting SOA mass after considering OrgNO_3 loss by hydrolysis. $[\alpha\text{-pinene}]_{\text{SS}} = 0.9$ to 2.2 ppb, $[\text{NO}_x]_0$ up to 125 ppb, $[\text{NO}_x]_{\text{SS}} = 0.3$ to 74 ppb. The effect of hydrolysis of 80% of the organic bound nitrate has no substantial effect on the SOA mass.